Technical University Munich
Physics Faculty

Bachelor Thesis in Physics

The Contribution of local Cosmic Ray Interactions to IceCube Neutrino Measurements

David Markus Kaltenbrunner
Matriculation Number: 03675833

14 December 2018

Max Planck Institute for Extraterrestrial Physics

Acknowledgements

This thesis is based on the research I did during my time at the Max Planck Institute for Extraterrestrial Physics as part of the Bachelor education I underwent at the Technical University of Munich. Towards both of these institutes I want to express how grateful I am for being able to get this experience and for helping me on my way towards the physicist I want to become. Also I want to thank Roland Diehl, Jochen Greiner, the whole group and Thomas Siegert for warmly taking me in. Especially Thomas, who not too seldomly spent hours to explain me what I actually was doing, deserves my gratitude. Last but not least of course I also want to thank my family and friends for always rebuilding my motivation during my work when it eventually dropped.

Abstract

The recently detected multi-messenger event of the blazar TXS 0506+56, flaring in ultra-high-energy (UHE) gamma rays and neutrinos at a high temporal correlation supports the theory blazars being important origins of neutrinos at energies above 10 TeV. First this suggestion came up when the IceCube collaboration announced the UHE neutrino flux to be isotropic rather than being dominated by events within the galactic plane as one would expect from sources like supernova remnants distributed within the Milky Way. This thesis presents an alternative way of testing and quantifying the isotropy of the neutrino flux by performing an expansion in spherical harmonics. In addition, it is shown that cosmic ray collisions with matter in the envelope of the Local Bubble, surrounding the Sun and its closest neighbours, to be another plausible explanation for neutrinos at such high energies. The latter is performed by calculating the neutrino and gamma ray flux one would expect from cosmic ray interactions within different length scales reaching from several tens of km to several Mpc. In this thesis, the inelastic proton-proton cross section of cosmic rays with ambient material is used to estimate neutrino and gamma-ray production rates in different interstellar media, characterised by their density and dimension. The resulting spectra are compared to IceCube data and show that the closest interaction regions for cosmic rays up to the distance to one of the closest Active Galactic Nuclei (AGN), Centaurus A, would already outshine the presumed population of AGN sources.

Abstract - Deutsch

Das Multi-Messenger Event, bei dem der Blazar TXS 0506+56 für kurze Zeit sowohl in ultrahochenergetischen Gammarays als auch Neutrinos einen verstärkten Fluss aufwies, hat dieses Jahr die These, Blazare könnten eine wichtige Quelle für Neutrinos dieser Energien darstellen, massiv gestärkt. Erstmals kam diese Idee auf, als die IceCube Kollaboration vor etwa fünf Jahren veröffentlichte, dass Neutrinos mit Energien höher als 10 TeV isotrop über den ganzen Himmel verteilt auftreten, was Supernova Remnants, welche einen Fluss vorwiegend in der galaktischen Ebene erzeugen würden, als starke Quelle unwahrscheinlich macht. Diese Arbeit präsentiert zum einen eine alternative Art, die Isotropie zu testen und zu quantifizieren, indem die Verteilung in Kugelflächenfunktionen entwickelt wird. Zum anderen wird auch gezeigt, dass Kollisionen von hochenergetischen Kosmischen Strahlen mit ruhender Materie in der Hülle der Local Bubble, welche die Sonne und nahe gelegene Sterne umschließt, einen nennenswerten Beitrag im relevanten Neutrinoenergiebereich ausmachen können. Dies wird durchgeführt, indem das Neutrino und Gamma Spektrum für verschiedene Längenskalen von mehreren km bis einigen Mpc bestimmt wird. In dieser Arbeit wird der inelastische Proton-Proton Wirkungsquerschnitt von Cosmic Rays mit umgebender Materie verwendet, um die Neutrino- und Photonenproduktionsraten in verschiedenen interstellaren Media, charakterisiert durch vorherrschende Dichten und ihre Ausdehnungen, abschätzen zu können. Die resultierenden Spektra werden mit IceCube Daten verglichen und zeigen, dass schon die nächsten Wechselwirkungsregionen für Cosmic Rays bis zum Abstand zu einem der nähesten Aktiven Galaxiekern (AGN), Centaurus A, einen höheren Neutrinofluss erwarten lassen als er für AGN Quellen gemutmaßt wird.

Contents

List of Figures

List of Tables

Neutrinos, they are very small
They have no charge and have no mass
And do not interact at all.
The earth is just a silly ball
To them, through which they simply pass,
Like dustmaids down a drafty hall
Or photons through a sheet of glass.
They snub the most exquisite gas,
Ignore the most substantial wall,
Cold-shoulder steel and sounding brass,
Insult the stallion in his stall,
And, scorning barriers of class,
Infiltrate you and me! Like tall
And painless guillotines, they fall
Down through our heads into the grass.
At night, they enter at Nepal
And pierce the lover and his lass
From underneath the bed-you call
It wonderful; I call it crass.

-John Updike

1

Introduction

For 9 years, the IceCube Neutrino Observatory (Aartsen et al. 2017c, Ahlers and Halzen 2014) located on and in an Antarctic glacier, has taken data on neutrinos. The facility measures energy and incident time based on Cherenkov light as well as time of the incident (Aartsen et al. 2017c). Especially the ultra high energy (UHE) part ($> 10\,\mathrm{TeV}$ neutrino energy) has brought up a lot of questions concerning its origins because the angular distribution is found isotropic (Aartsen et al. 2014, The IceCube Collaboration et al. 2015) and the flux higher than expected from interactions of cosmic rays with our atmosphere (Aartsen et al. 2017a). This isotropy suggests either very close range events below 400 pc meaning within or close to the boundaries of our Local Hot Bubble (Slavin 2017, Lallement 2015, Lallement et al. 1998) or a population of distance sources at cosmological scale (AGN). Were the main sources of the neutrinos supernova (SN) remnants only within our galaxy, i.e. below tens of kpc, the neutrinos would mainly originate from low galactic latitudes, only from the galactic disc (The IceCube Collaboration et al. 2015).

One possible origin of such UHE neutrinos are thought to be blazars. Due to a recent multi-messenger event of the source TXS 0506+056, the popularity of investigating especially this kind of origin increased a lot. TXS 0506+056 has been detected to emit an increased flux in UHE gamma-rays while also being the first ever detected point source for neutrinos in this energy realm (IceCube Collaboration et al. 2018a, IceCube Collaboration et al. 2018b). Since AGN generally are spread across the sky in an isotropic way, they make for a fitting explanation for a big part of UHE neutrinos in general (e.g. see map 2.10 from Aartsen et al. 2017b containing 862 AGN spread isotropically over the sky).

Another possible source of these neutrinos is believed to originate from cosmic ray (CR) interactions in the dense material creating the wall between the Local Bubble and the L1 Bubble with the cosmic rays originating from a single supernova remnant (SNR) within the L1 Bubble (Andersen, Kachelriess and Semikoz 2018).

This thesis will explore contributions from CR-interactions in varying media/conditions as a function of distance from the Sun to a theoretical neutrino and gamma-ray flux and compare the results with data from experiments measuring the diffuse spectra.

Chapter 2 summarizes neutrino physics, cosmic ray physics and the connection to the interstellar medium. Origins for different parts of the neutrino and cosmic ray spectra as well as structures in the interstellar medium and approximate values for density in these up to distances of several Mpc are explained.

In chapter 3 particle detection basics as well as various experiments utilizing these will be presented. The experimental set-up of the IceCube detector will be explained and discussed in detail.

Next chapter 4 has its scope on the mathematical foundation, considering interaction kinematics and cross section and explains the resulting spectra. The used cosmic ray model for this analysis is explained and the resulting gamma-ray and neutrino fluxes are shown together with an analysis of IceCube data.

Chapter 5 will then discuss the outcome of the calculations concerning plausibility, to which degree the assumptions hold and how big the contribution to the flux calculated in this way

would be expected. At the chapter's end there will be a short section about the possibility of utilizing neutrino oscillations for distance measurements, which would be useful to determine the true sources of neutrinos.

All of this will then be summarized in chapter 6 and a prospect of what might be possible in the future will be given.

2

Astro- and Particle-Physics

> *In the beginning the Universe was created. This has made a lot of people very angry and been widely regarded as a bad move.*
>
> – Douglas Adams

Humankind has found a source of fascination in the night sky since the very first day. Once Earth turns far enough for the Sun not to predominate due to its massive brightness any more, one's sight is free to wander towards places, way too distant to be conceivable compared to distances one knows, towards times, aeons of years past. One can watch hundreds and thousands of stars and galaxies, many of which we don't even know yet to have ended their nuclear fusion stage in tremendous supernova explosions already long ago. And this becomes possible simply because the 'noise' caused by the Sun on the 'signal' of one's vision is switched off and our 'instruments' our eyes are able to get more sensitive. On the first glance though the only thing to happen is that one suddenly mysteriously gazes at beautifully sparkling bright dots on a dark sky. And as much as humans love mysteries, as strong is the desire to solve them or at least to find an explanation that many can agree on. Exactly this desire is the driving force behind science, the reason for humans to keep going thinking about better ways to observe. What started as dreamily watching the sky slowly became taking notes of on what paths celestial bodies move, examining them with telescopes and reached building incredibly huge facilities and sending satellites and spacecraft into space for being able to measure things far beyond human vision. Since by now there are multiple ways of observing celestial bodies, multi-messenger astronomy became crucial. First it enables testing theories about processes not accessible in any other way, secondly, it's not always that easy to determine the origin of any signal as it is for visual light. Just this fact makes it such a monumental event for scientists, being able to announce the first multi-messenger event of a kind, like it happened for gravitational waves and gamma-rays in 2017 (Abbott et al. 2017) and neutrinos and gamma-rays in 2018 (IceCube Collaboration et al. 2018a, IceCube Collaboration et al. 2018b). The scope of this thesis is to find a connection between ultra high energetic neutrinos measured by the IceCube laboratory, cosmic rays surveyed with diverse instruments for example on satellites or balloons, gamma-rays, that always appear in processes that are supposed to form these neutrinos, and densities of the interstellar medium measured through X-rays. To properly discuss the link between these measurements, why the data provided by IceCube are that startling and to which degree it could be associated with those other observations, this chapter cover the fundamental knowledge needed.

2.1 Neutrino Physics

This section provides the basics about neutrinos. For a better understanding what makes them special and mysterious particles to many, as a start a little history on how the need for the existence for such a particle came up, how it was first verified and the search for their characteristics proceeded.

2.1.1 A little History on Neutrinos

1930 - The very year that neutrinos got postulated by Wolfgang Pauli in a famous letter he wrote to the so called 'Gruppe der Radioaktiven'. At this time physicists thought there to be three unresolvable elemental components of the universe: electrons, protons and photons. One big issue back then though was the electron energy spectrum for β decays measured by Lise Meitner and Otto Hahn, that was contrary to expectations continuous rather than discrete as it should be for a decay into the two particles that had been detected. The problem was that a continuous spectrum in a two body decay violates the laws of energy and momentum conservation. Unlike Niels Bohr's idea, conservation laws could be understood in a statistical way, Pauli proposed an additional particle he called 'neutron', that had not been measured during the experiment and carrying the missing energy and momentum from the decay. However, the particle he proposed in terms of characteristics neither was the nowadays neutron nor was it the neutrino but rather a mixture of both. The name 'neutrino' first emerged due to the Italian physicist Enrico Fermi out of a wordplay he made due to its low predicted mass (neutrone in Italian meaning big and neutral, neutrino small and neutral; Brown 2008).

Fermi, who was fond of this idea of a new particle explaining missing energies started working on a theory to explain what Pauli had suggested, the theory on weak interactions he presented already 1934. However, it took more than two decades to finally being able to create an experiment to draw on. Cowan et al. 1956 provided evidence for the existence of neutrinos by detecting neutrinos emitted by a nuclear reactor in the Cowan-Reines Neutrino Experiment.

After in 1936 the muon had been first detected and in 1937 its existence had been proven (Street and Stevenson 1937) in 1962 its neutrino counterpart, that's existence had been predicted in the late forties with the idea of lepton family conservation, was found (Anicin 2005). In 1968 R. Davis, D. S. Harmer and K. C. Hoffman managed to first measure solar neutrinos using a 380000 litre tank of perchloroethylene with J. N. Bahcall doing the theory and calculations behind the experiment (Davis, Harmer and Hoffman 1968) and thereby prove the validity of the theory, the Sun to be powered by nuclear fusion reactions (Davis and Bahcall 1969). However a lower neutrino rate than expected was measured. A few years later the third and to date last left lepton family was found with the tau particle by M. L. Perl at the SLAC-LBL group indirectly through the interaction

$$\mathrm{e}^+ + \mathrm{e}^- \rightarrow \mu^\pm + \mathrm{e}^\mp$$

plus at least two undetected particles to meet the family number conservation law. (Perl et al. 1975)

After this the era of huge neutrino experiments began. In 1982 the IMB experiment started operating, in 1983 Kamiokande followed. One of their first major discoveries was the detection of neutrinos from the very close supernova SN 1987A in the Large Magellanic Cloud - one of the closest satellite galaxies of the Milky Way - by IMB, Kamiokande and Baksan which marked the birth of neutrino astronomy. (Arnett et al. 1989)

Shortly after, in 1989, Kamiokande manages to be the second experiment to detect solar neutrinos while at the same time as well finding the measured neutrino flux to be way lower than expected from models (Davis, Mann and Wolfenstein 1989). During the following years several experiments published data that all led towards a conclusion that a non-zero mass for neutrinos would be the easiest way to explain differences between theory and experiments for only this permits flavour oscillations between neutrinos, a process similar to the one of neutral particles like $\mathrm{K}^0 - \bar{\mathrm{K}}^0$ or similar mesons. Finally in 1998 the Super-Kamiokande Collaboration brought up evidence for neutrino oscillations and thus for the fact that neutrinos indeed have mass (Totsuka and Super-KAMIOKANDE Collaboration 1998). Since then physicists all over the world try to measure this mass or at least mass differences between different flavours by various kinds of experiments.

Another big issue started in 1996 when the AMANDA neutrino telescope began operating by utilizing big volumes of Antarctic ice together with photomultipliers to measure Cherenkov radiation from neutrino induced events (see chapter 3]). AMANDA together with its successor IceCube and also other experiments using liquid water like in the Mediterranean Sea or at Lake Baikal enabled the means to detect neutrinos to energies way beyond experiments like Kamiokande, that were bound by the man-made apparatus' size. Through these it was found that a big part of ultra high energy neutrinos (above 10 TeV) are likely to have extra-galactic origins with blazars being one of them. This topic will be discussed in more detail in chapter 5.

2.1.2 Primary Characteristics

> *Neutrinos...win the minimalist contest: zero charge, zero radius and very possibly zero mass.*
>
> – Leon M. Ledermann

Neutrinos are fermions, meaning they have half integer spin, more specific leptons, hence not being affected by strong interaction.

As stated by L. Ledermann: The three neutrino flavours currently known are very small and light with no charge and thus only weakly interacting particles. In absence of knowledge whether those three flavours are the only ones existing, often they are referred to as 'light neutrinos' with their heavy counterparts being predicted to have masses not accessible with experiments at present. The suggestion of neutrinos having heavy correspondents is induced by the fact that the electron, muon and tau neutrino have masses at the order of meV to eV while other elementary particles typically have masses at the order of keV to GeV. However, different to most other particles it's also very difficult to exactly determine neutrinos' masses. Only upper limits as well as mass differences between flavours, both at the order or eV (concluded from neutrino oscillations, see section 2.1.6) are known to date (Povh et al. 2014).

2.1.3 Weak Interactions

Together with gravitation, coulomb (electromagnetic) and strong interaction, the weak force makes the fundamental forces we use for describing our universe. Except for gravity these forces are being mathematically specified by and linked with each other via the Standard Model of particle physics (SM). In addition the electromagnetic and the weak interaction are described as two aspects of the electroweak interaction that become evident due to the Higgs Mechanism. Within the Standard Model all forces are carried by gauge bosons (electromagnetic by photon, strong by gluons and weak by Z^0 and $W^{\pm}$), that together with the specific coupling constants define the strength and probability of interactions. Different to photons and gluons, that are massless, the Z^0 and $W^{\pm}$ with masses of nearly $100\,\mathrm{GeV/c^2}$ are close to the top of elementary particles found to date. This leads to low cross sections and also makes the weak force very short ranged such that (different to Coulomb or gravitational interactions) it seems to taking place on a single Point (Povh et al. 2014).

Talking about weak interaction one distinguishes between charged and neutral current. This means the interaction can be explained via a W-Boson transfer or the one of a Z-Boson. In figure 2.1 one can see, what the difference between these interactions is.

Another aspect about weak interaction that makes it special is that it influences left- and right-handed particles and antiparticles in different ways. Charged current for example only affects left-handed particles and right-handed antiparticles. This leads to pions rather decaying into muons than directly into electron (cf. section 2.1.4).

However, a complication in determining the characteristics of weak interactions there is that due to it's low relative strength[1] (Halzen and Martin 1984) its effects are mostly covered by the other two SM forces at scattering experiments. Thus examining β decays is the main way to find weak interaction properties.

2.1.3.1 Fermion Families

The standard model of particle physics describes all matter as 12 structureless fermions class-divided into six families. Leptons and quarks each consist of three of these families called the three generations. In table 2.1 this subdivision is shown.

Table 2.1: *Fermions paired in families of 1st, 2nd and 3rd generation with charge Q* (Anicin 2005)

	$1st$	$2nd$	$3rd$	Q
Quarks	$\begin{pmatrix} \mathrm{u} \\ \mathrm{d'} \end{pmatrix}$	$\begin{pmatrix} \mathrm{c} \\ \mathrm{s'} \end{pmatrix}$	$\begin{pmatrix} \mathrm{t} \\ \mathrm{b'} \end{pmatrix}$	$+2/3$
				$-1/3$
Leptons	$\begin{pmatrix} \nu_\mathrm{e} \\ \mathrm{e}^- \end{pmatrix}$	$\begin{pmatrix} \nu_\mu \\ \mu^- \end{pmatrix}$	$\begin{pmatrix} \nu_\tau \\ \tau^- \end{pmatrix}$	0
				-1

The reason for all down-like quarks being primed is that they experience strong interactions and their strong (or mass) eigenstates down (d), strange (s) and bottom (b) are mixing into their weak eigenstates d', s' and b' via the CKM (Cabibbo-Kobayashi-Maskawa) transformation matrix.

Due to the reason that leptons don't experience strong interactions there is no need for a mixing like there is for quarks.

2.1.3.2 Conservation Laws

Interactions in general are conventionally illustrated using Feynman Diagrams consisting of vertices (connection points), virtual particles (internal lines) and real particles (external lines). However, these Diagrams are not just illustrations but in fact are a type of notation for the mathematics describing the process. Thus, at each vertex all conservation laws applying to the interaction taking place at it must be met. What quantities are conserved during weak interactions can be explained using figure 2.1. For weak interactions the exchange particles for energy and momentum are the bosons Z^0, W^+ and W^-.

First it is important to mention what conservation means for calculations with and discussions about Feynman Diagrams. Usually they are read from bottom to top in time and from left to right in spatial propagation, which will also be used within this thesis. However, these two axes can be exchanged. Whatever conserved quantity is carried towards a vertex must be carried out from particles emerging from it. Another norm is, that arrows for antiparticles (usually) are drawn in the opposite direction of their spatial and time propagation (not the case in figure 2.1; Povh et al. 2014; Grotz and Klapdor 1989).

In SM weak interactions, energy, momentum, angular momentum charge, lepton number and baryon number are conserved. Except for neutrino oscillations, lepton family number has been found to be conserved too. Even though these are not many there do come up interesting effects. This for example is important in the course of this thesis for pion decay.

[1] In comparison electromagnetic interaction is stronger by a factor of about 10^8, strong interaction by around 10^{11}. These numbers of course are dependent on the energy regime the interaction takes place in.

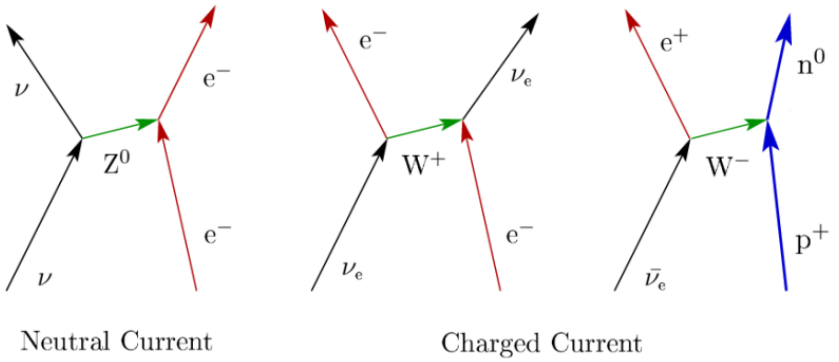

Figure 2.1: *Interaction between neutrinos and matter to accelerate/create electrons; from left: via neutral current with electron, via charged current with electron and via charged current with neutron; propagation in time follows the vertical direction and in space the horizontal direction*

Pions are spinless and the lightest hadrons, thus only having the possibility of decaying into an electron or muon and an antineutrino of the same lepton family. This has to happen via the charged current, which only couples to left-handed particles and right-handed antiparticles. For the antineutrino (neutrino) this means that spin and momentum have to be parallel (antiparallel). In the rest frame of the pion due to conservation of momentum and angular momentum (which initially are 0) the same must be true for the charged lepton. If it were at the speed of light, this particle now would also be right-handed, which is not allowed due to it interacting with a W-Boson. For non-relativistic particles however, chirality and helicity are different from one another. A right-handed particle becomes a superposition of one with positive and negative helicity. This makes it possible for the muon to have a positive helicity and still being left-handed. (Povh et al. 2014)

2.1.4 Where do they come from...

In this thesis two ways to look at where neutrinos come from are explained. First I will explain what interactions are most likely to form neutrinos in general, and in the second part I give locations these interactions take place at and what neutrino energies result from them. Both will be explained during this chapter together with figure 2.2 that shows what fluxes are expected or measured coming from different sources.

2.1.4.1 Particle Physics Interactions

A prominent source of neutrinos is represented by transitions between neutrons and protons. There are different processes during which this happens: β^+ and β^- decay as well as electron capture. During a β^+ decay a proton within a nucleus decays into a neutron, a positron and an electron neutrino which forms a different elements, for example:

$$^{101}_{46}\mathrm{Pd} \rightarrow ^{101}_{45}\mathrm{Rh}^- + \mathrm{e}^+ + \nu_\mathrm{e}.$$

Due to the fact that the neutron rest mass is higher than the proton's, this decay can only take place within a nucleus where the mass of the product is sufficiently smaller than that of the parent atom. Its counterpart is the β^- decay, where a neutron becomes a proton, an electron and an electron antineutrino. This also is what happens to a free neutron.

In an electron capture process, an electron from a K or L shell is absorbed by a nucleus proton to form a neutron and an electron neutrino according to

$$\mathrm{p}^+ + \mathrm{e}^- \rightarrow \mathrm{n}^0 + + \nu_\mathrm{e}.$$

This is most likely to happen to very heavy nuclei for their inner shells' electron have a high probability to be located within the nucleus due to how their wave functions look like and how big the nuclei already are. Electron capture is an alternative to a β^+ decay when the energy difference between parent and daughter nucleus is low. After the electron capture, because of an electron in an inner shell is missing, the atom emits characteristic X-rays while electrons from outer shells cascade down (Povh et al. 2014).

The second important source of neutrinos are decays of charged mesons that occur for example due to collisions of nuclei. However, since these mesons (as mentioned in section 2.1.3.2) are most likely to decay into muons and them not being stable the decay chain contains three emerging neutrinos as in

$$\pi^+ \rightarrow \mu^+ + \nu_\mu \rightarrow \mathrm{e}^+ + \bar{\nu_\mu} + \nu_\mu + \nu_\mathrm{e}.$$

A process where only neutrinos emerge from is the pair production of a neutrino and its antineutrino. This can happen due to an annihilation process (for example of an electron and a positron) with a Z^0 as the exchange particle instead of a photon. However, due to the high rest mass of the Z^0 this process is highly suppressed compared to others.

2.1.4.2 Astrophysical Sites

Figure 2.2 show ranges of intensities of neutrino flux from different astrophysical and terrestrial sites and gives an idea of relative flux intensities within different energy regimes.

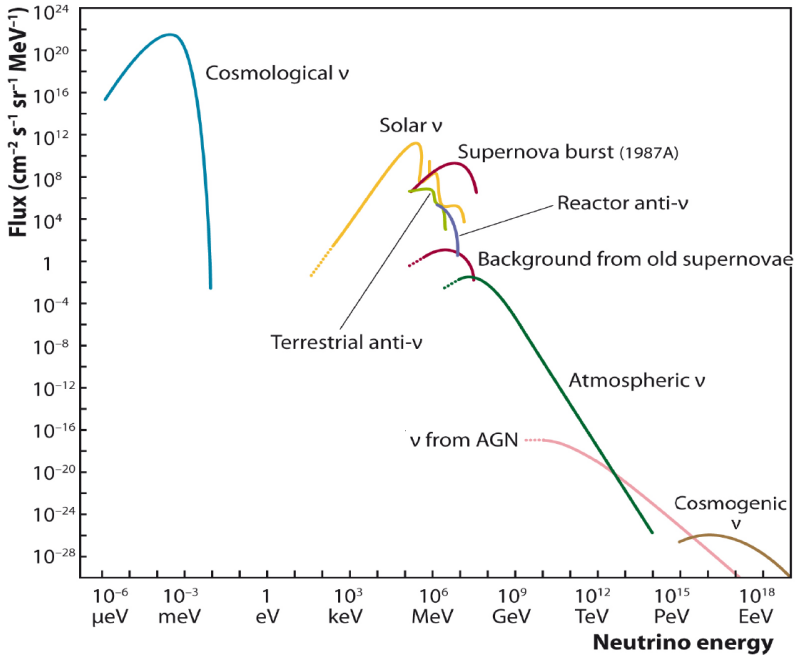

Figure 2.2: *Neutrino flux ranges over energy in eV (Joutsenvaara 2016)*

Starting at low energies the by far highest flux comes from cosmological ν, similar to the cosmic microwave background (CMB). It is seen as a relic of the Big Bang as well and consists of neutrinos that due to expansion of space were redshifted towards energies around μeV and meV (Follin et al. 2015).

The next source by flux are solar neutrinos ranging from keV to MeV. They originate from various fusion reactions taking place in the Sun, the biggest part from

$$\mathrm{p}^+ + \mathrm{p}^+ \rightarrow^2 \mathrm{H}^+ + \mathrm{e}^+ + \nu_\mathrm{e}$$

where $^2H^+$ is a deuteron, but also decays arising from unstable nucleons forming and decaying during the fusion processes (for example ^8B). There are steps inside of the solar neutrino spectrum due to different reactions having different maximum energies but all of them being continuous spectra instead of sharp peaks due to them being 3-particle-decays (Bellerive 2004).

The supernova SN 1987A was a transient source and could only be seen for a short time. These neutrinos are supposed to emerge at the time of the core collapse during the supernova. This means that different to photons, which cannot escape at these times due to the stars outer layers being opaque to them, they can tell us what happens during a supernova in more detail. The energies measured are comparable to terrestrial neutrinos (either from decaying elements within Earth or from reactors) to the neutrinos expected from the diffuse supernova neutrino background. Since it is supposed to being caused by supernovae all over the sky too dim to be seen as sources, this only is a logical assumption (Billard, Figueroa-Feliciano and Strigari 2014; Arnett et al. 1989).

Interactions in our atmosphere to form neutrinos are supposed to be similar to the ones causing active galactic nuclei (AGN) to emit them. The only difference is where these interactions take place. Both of them are about high energetic particles colliding with ones being nearly at rest, creating high energy mesons that decay into leptons and photons. Either cosmic rays hit particles in our atmosphere or they already interact with the cold gas surrounding the AGN or any other particle accelerator[2]. Even though the reactions are believed to be the same, due to the cosmic rays having to travel through the intergalactic medium for being able to interact with our galaxy, the spectra are believed to have different power laws (Murase 2015). However, the atmosphere is not the only close by matter that cosmic rays can interact with to form neutrinos but also other high density regions like the envelope of the Local Bubble (cf. section 2.3) might be relevant. Since this concept is the main idea behind this thesis, section 2.1.4.3 explains the basic principle of high energy neutrinos emerging from cosmic ray interactions. How big the contribution of this process happening in the local interstellar medium media to the total neutrino flux is, is not clear a priori.

Finally at very high energies of PeV to EeV there are neutrinos predicted to emerge due to the Greisen-Zatsepin-Kuzmin limit. Cosmic rays above a certain energy have the possibility to interact with CMB-photons via the Δ resonance creating high energy pions and thus again high energy neutrinos and photons (Watson 2014).

2.1.4.3 Processes to form Neutrinos and Photons

Why are cosmic rays important for and how can they be associated with neutrino and gamma measurements. The high energy neutrinos this thesis' scope is, mainly originate during decays of high energy mesons. These mesons form during inelastic interactions between cosmic rays and (interstellar proton) gas (pp interactions) or between protons with CMB photons ($p\gamma$ interactions). However, during these interactions not only high energetic neutrinos but also photons are created. This happens due to the fact that besides charged mesons there always are neutral ones occurring in these processes at similar rates. The neutral mesons then decay into photons which will be part of the gamma-ray spectrum (Kelner, Aharonian and Bugayov 2006).

At start the photons and neutrinos have very similar spectra with the same slope and a relation which is approximately given by $E_\gamma^2\phi(E_\gamma) = 2E_\nu^2\phi(E_\gamma)$. Though, when travelling cosmological distances these very high energy (VHE) photons interact either with CMB photons via electromagnetic (EM) cascades or with matter of the interstellar medium to sub-TeV photons (de Angelis et al. 2009). Through high sensitivity measurements of gamma spectra for example by

[2]Supernova remnants are being discussed as one of them, though no neutrinos in the UHE regime that were detected by experiments like IceCube could have been associated with galactic point sources by now (cf. chapter 5).

Fermi (see chapter 3) thus constraints on sources of high energy neutrinos can be made (Mészáros 2017).

Kelner, Aharonian and Bugayov 2006 gives profound calculations of these interactions using simulation data from the public available SIBYLL code in order to obtain approximations for meson, photon and lepton spectra with a given cosmic ray energy distribution. What assumptions are made for being able to calculate the fluxes and what formulae and results arise from those will be explained in chapter 4. The exact formulae (originally described in Kelner, Aharonian and Bugayov 2006) will be shown and briefly explained in appendix B.

2.1.5 ...and where do they go?

The theory behind what fluxes we expect from different celestial objects is not a prove for these fluxes actually passing through. Neutrinos detected by their secondaries which interact electromagnetically. In the following these possibilities, how these secondaries can be formed, are covered. In chapter 3 experiments utilizing these interactions will be explained.

2.1.5.1 Neutral Current versus Charged Current

The Z^0 interaction will lead to no change in particle identities (left one in figure 2.1). All neutrino flavours have the same probability to interact with a specific particle this way and the second particle will only be accelerated, thus due to conservation of energy and momentum the highest effect is obtained against low mass counterparts like an electron. A core interacting with a neutrino this way will barely move at all (Povh et al. 2014).

Due to the fact that there mostly are electrons around and close to no other charged leptons or antileptons only neutrinos and no antineutrinos can be observed through interactions similar to the middle one in figure 2.1. Still all three neutrino flavours can interact with an electron which leads to either a fast electron, muon or tau departing from the place of incident (Povh et al. 2014).

The last shown event is a neutrino induced beta decay with two detectable products, a fast charged lepton and a core with its atomic number changed due to converting a neutron into a proton or vice versa (Povh et al. 2014).

Another relevant interaction, that is not shown is the scattering of an electron antineutrino on an atomic electron, from which via a W^- either a negatively charged lepton with its antineutrino or an antiup-like and a down-like quark ending in a shower emerge (IceCube Collaboration 2013).

2.1.5.2 Cross Section

In a scattering experiment the number of scattered particles I_s can be calculated as the product of cross section σ, number of incident particles I_i and the surface density of the target λ according to

$$I_s = \sigma \lambda I_i.$$

Thus the cross section characterizes the probability of an interaction taking place in a medium (higher cross section means higher probability). For example muon neutrinos at 100 GeV interacting with nuclei via the charged current have a cross section at the order of $1\,\mathrm{pb} = 10^{-40}\,\mathrm{m}^2$ (Tanabashi et al. 2018). The cross section for inelastic proton-proton scattering at this energy in comparison is approximately $10\,\mathrm{mb} = 10^{-30}\,\mathrm{m}^2$ (Kelner, Aharonian and Bugayov 2006).

2.1.6 Flavour Oscillations

It has been shown, that neutrinos oscillate between flavours (Totsuka and Super-KAMIOKANDE Collaboration 1998). The only way for this to be explained by a theoretic model is by neutrinos

having a rest mass, and their mass eigenstates (ν_1, ν_2 and ν_3) not coinciding with their weak eigenstates (ν_e, ν_μ and ν_τ). Mass eigenstates in general define how particles propagate through space and time, neutrinos' weak eigenstates are the ones we can actually detect through their interaction with matter. Flavour eigenstates now can be written as a linear combination of ν_1, ν_2 and ν_3 with the unitary matrix U - called PMNS-Matrix - as in equation 2.1. Bra-ket notation is used to define the state of neutrinos here (Povh et al. 2014).

$$\begin{pmatrix} |\nu_e\rangle \\ |\nu_\mu\rangle \\ |\nu_\tau\rangle \end{pmatrix} = U \cdot \begin{pmatrix} |\nu_1\rangle \\ |\nu_2\rangle \\ |\nu_3\rangle \end{pmatrix} \tag{2.1}$$

U in this equation is given as

$$\begin{pmatrix} c_{12}c_{13} & s_{12}c_{13} & s_{13}e^{-i\delta} \\ -s_{12}c_{23} - c_{12}s_{23}s_{13}e^{i\delta} & c_{12}c_{23} - s_{12}s_{23}s_{13}e^{i\delta} & s_{23}c_{13} \\ s_{12}s_{23} - c_{12}c_{23}s_{13}e^{i\delta} & -c_{12}s_{23} - s_{12}c_{23}s_{13}e^{i\delta} & c_{23}c_{13} \end{pmatrix} \begin{pmatrix} e^{i\alpha_{21}/2} & 0 & 0 \\ 0 & e^{i\alpha_{31}/2} & 0 \\ 0 & 0 & 1 \end{pmatrix}$$

where $c_{ij} = \cos\theta_{ij}$ and $s_{ij} = \sin\theta_{ij}$ with the mixing angles $\theta_{23} \approx \pi/4$, $\theta_{12} \approx \pi/5.4$ and $\theta_{13} \approx \pi/20$ (Tanabashi et al. 2018). δ is the Dirac CP violation phase, α_{21} and α_{31} are the Majorana CP violation phases (cf. Povh et al. 2014). Currently the only known of these three phases is $\delta \approx 3\pi/2$. During calculations for this thesis the others are set to 0. They do have a small influence on what we expect but not to an amount that it fundamentally changes what we observe (Tanabashi et al. 2018).

For simplicity the following explanation of neutrino oscillations considers two flavours. Their mass eigenstates ν_1 and ν_2 are mixing into the weak eigenstates ν_α and ν_β with a mixing angle θ as

$$\begin{pmatrix} |\nu_\alpha\rangle \\ |\nu_\beta\rangle \end{pmatrix} = \begin{pmatrix} \cos\theta & \sin\theta \\ -\sin\theta & \cos\theta \end{pmatrix} \cdot \begin{pmatrix} |\nu_1\rangle \\ |\nu_2\rangle \end{pmatrix}.$$

Now let's assume to have a pure $|\nu_\alpha\rangle$ at the start. Propagation can be described via the neutrino's time dependent wave function as

$$|\nu_\alpha(t)\rangle = \cos\theta \exp\left(-\frac{iE_1 t}{\hbar}\right)|\nu_1\rangle + \sin\theta \exp\left(-\frac{iE_2 t}{\hbar}\right)|\nu_2\rangle$$

where $\hbar$ is the reduced Planck's constant and E_1 and E_2 are the mass eigenstate energies only different due to their different masses. Because of pc (with the momentum p equal for both eigenstates; vacuum speed of light c) being much larger than mc^2 one could approximate the energies by pc. However, this way the equation would be independent on the mass eigenstates and no oscillations are possible, which is why for the first step the more accurate approximation

$$E_i \approx pc\left(1 + \frac{1}{2}\frac{m_i^2 c^4}{p^2 c^2}\right)$$

is necessary. Using that neutrinos travel approximately at the speed of light one can write the distance travelled as $L = ct$. With this the probability of detecting neutrino ν_x (x either α or β) is given as $P_{\nu_\alpha \to \nu_x} = |\langle \nu_\alpha(t)|\nu_x\rangle|^2$. Since $|\nu_1\rangle$ and $|\nu_2\rangle$ are orthonormal states ($\to \langle\nu_1|\nu_2\rangle = 0$) exemplary the probability for detecting ν_α at given L is

$$P_{\nu_\alpha \to \nu_\alpha} = 1 - \sin^2 2\theta \sin^2\left(\frac{1}{4}\frac{\Delta m_{\alpha\beta}^2 c^4}{\hbar c}\frac{L}{pc}\right)$$

where for pc the neutrinos energy can be used (Povh et al. 2014).

This very same principle can be used for three flavours as well. Given this only one more information is needed in order to calculate how neutrinos oscillate, the mass square differences $\Delta m_{ij} = m_i^2 c^4 - m_j^2 c^4$. As a best fit of $\Delta m_{21} = 7.37 \cdot 10^{-5}\,\mathrm{eV}^2$ was found. However, experiments were not able to determine, whether m_3 is larger or smaller than the other two and only $|\Delta m| = |m_3^2 c^4 - {}^{(m_2^2 c^4 + m_1^2 c^4)}/_2|^2 = 2.50 \cdot 10^{-3}\,\mathrm{eV}^2$ was found (Tanabashi et al. 2018).

Figure 2.3 shows the outcome of these calculations for a prior neutrino flux of electron neutrinos at 10 TeV. Shown is the length scale at which the oscillations occur from 10^9 m to $25 \cdot 10^{10}$ m - corresponding to npc to μpc - on a logarithmic scale (on a linear scale oscillations would appear sinusoidal as one would expect from $P_{\nu_\alpha \to \nu_\alpha}$).

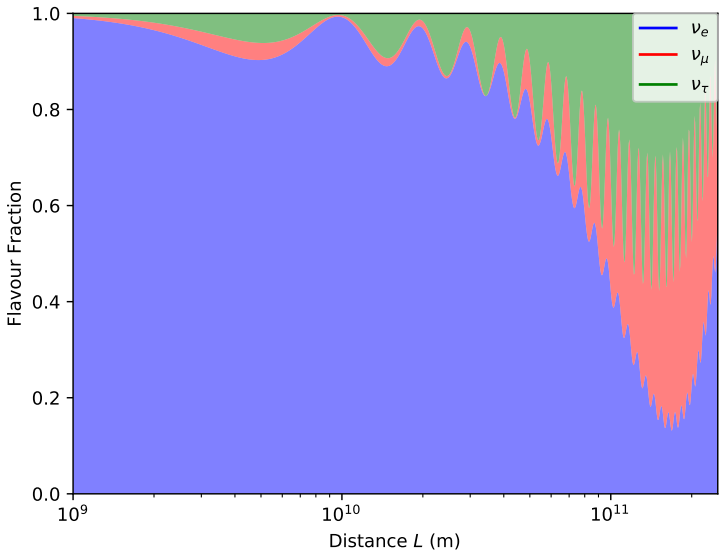

Figure 2.3: *Neutrino Oscillations: Flavour contribution plotted over distance from origin for a prior flux of 10 TeV electron neutrinos*

However, there is a second type of neutrino oscillation. When neutrinos propagate through matter their mass is increase corresponding to their interaction with it. Especially within the sun with a high electron density electron flavoured neutrinos gain mass due to their higher interaction probability than that of muon neutrinos. Thus the electron neutrino is closer to being $|\nu_2\rangle$ than in vacuum and the mixing angle changes. This alone does not cause any more oscillations yet. Only as soon as the neutrino travels into a less dense region due to constant change of mixing angle the oscillation probability increases a lot. This effect is called MSW mechanism (Wolfenstein 1979).

2.2 Cosmic Rays

Cosmic rays interactions are an important source for neutrinos, but what are these rays in the first place. CRs mainly consist of high energetic nuclei totally stripped off their electron shell (the biggest part are protons or alpha particles, a much smaller amount are heavier nuclei as well) and to a very small degree of free electrons.

2.2.1 How it began

At around 1900 people were experimenting with electroscopes, charge-based devices to measure ion density which can be used to provide evidence for ionising radiation. Back then only gamma-

rays coming from radioactive decays of earth crust elements were know for this behaviour and their absorption coefficient in air already were well studied. Finding that radiation did not fall off as much as expected puzzled physicists. T. Wulf was one of the first to document this effect, when in 1910 he measured way higher ion densities than there should have been at the top of Eiffel Tower compared to the ground. Since at this time gamma-rays were the most penetrating ionising radiations known but them having too high absorption coefficients to explain this, physicists assumed more penetrating gamma-rays coming from the sky. Hence experiments went further and further up, now using balloons. As a pioneer in this field V. F. Hess systematically measured the radiation up to altitudes of 5.3 km during 1911-1912. With the Geiger-Mueller detector invented in 1929 it was possible to examine time correlation between events. During the same year W. Bothe together with W. Kolhörster and B. Rossi using two Geiger counters and a strong absorber in between (for example a block of gold) found that cosmic rays most certainly consist of charged particles rather than gamma-rays (Longair 1981).

Starting in 1954 several experiments on balloons and later satellites too arose to measure the energy spectrum and arrival directions of cosmic rays using for example scintillation detectors or calorimeter. Modern experiments for analysing cosmic rays will be discussed in chapter 3.

2.2.2 Constituents

Cosmic rays mainly consist of nuclei and to a negligible degree of electrons and other particles. Conventionally there are five groups of nuclei that are treated separately, namely H (protons), He (alpha particles), CNO, Mg-Si and Mn-Fe. This grouping helps characterizing the energy spectrum by physically relevant parameters like particle energy and atomic number Z (Gaisser 2012).

2.2.3 Characteristic Energy Spectrum

Gaisser 2012 finds a fit to all particle data from various missions that can be seen in figure 2.4 where the black line is the sum of the five nucleus groups and was fitted to the data. Figure 2.5 shows a close-up on two important features of this spectrum, the 'Knee' and the 'Ankle', marking regions where different effects dominate the spectrum. The reason for the flux being multiplied by different powers of energy is for the characteristic features to be more apparent. Even small variations in spectral indices can be linked to different origins, thus the differentiation between them is important. In addition the measured fluxes at these energies are extremely low. Giving numbers: At energies of the Knee a detector with a size of $1\,\mathrm{m}^2$ is hit by one particle per year on average, at the Ankle energies a particle detector with $1\,\mathrm{km}^2$ in size is needed for similar count rates already (Bergström and Goobar 2006). Explicit information on which papers the data is taken from can be found in Gaisser 2012. Equation B.1 in the appendix gives the mathematical description of the cosmic ray spectrum for each of the five groups i with the parameters given in table B.1.

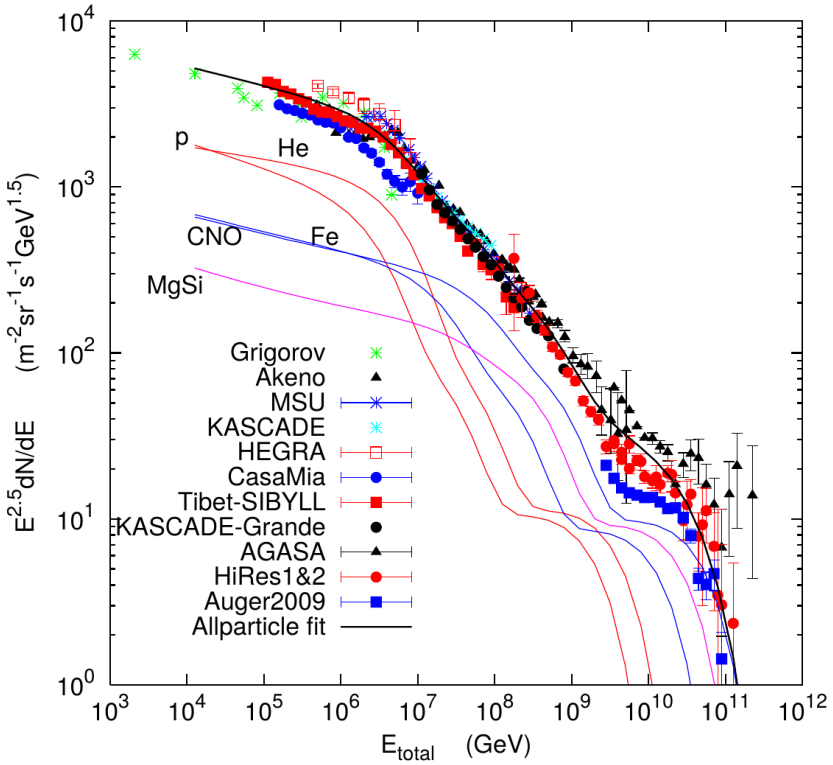

Figure 2.4: *Three-population model of the cosmic ray spectrum defined by equation B.1 compared to data (Gaisser 2012)*

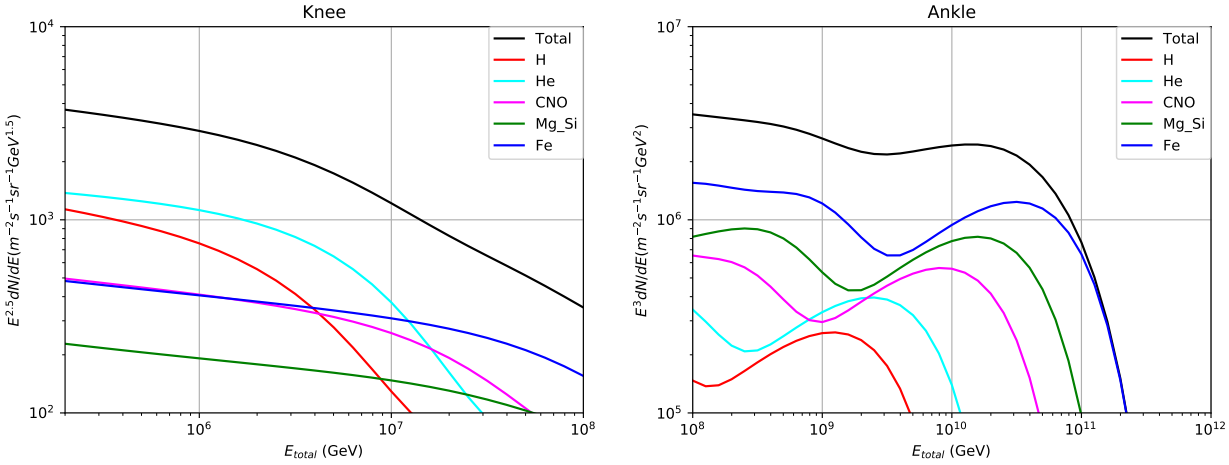

Figure 2.5: *Close-up of the so-called knee (left) and ankle (right) characteristics plotted using equation B.1*

2.2.4 Cosmological Origins

Here, it will be discussed how the spectrum as seen in figures 2.4 and 2.5 can be explained. Hillas 2006 and Gaisser 2012 describe the spectrum as three populations of different origins of acceleration. Classified by the integral spectral indices, the first population is linked to supernova remnants with the knee as its cut-off. The second is assumed to be of a galactic origin as well, even though it cannot be brought in correlation with any specific objects, for which reason it is

called 'Component B'. Finally the third component of highest energy at the ankle is associated with extra-galactic origins such as active galactic nuclei (AGN, also see chapter 5; Hillas 2006; Gaisser 2012).

2.3 The (Local) Interstellar Medium

Density distributions are the final fundamental part of the calculations in this thesis. Therefore, this section will have its scope on some findings about the local interstellar medium, reaching from our solar system to one of the closest AGN, important for this thesis.

2.3.1 Milky Way

> *The number of stars making up the Milky Way is about* 10^{11} *or something like the number of raindrops falling in Hyde Park in a day's heavy rain.*
>
> – Sir Jack Balwin

In his 'Siderius Nuncius' Galileo was the first one to ever describe the Milky Way as a resolvable stellar system. Even though around 1600 his means were very limited compared to modern telescopes which led to him only seeing the brightest stars, he made relevant observations like the existence of star clusters. Approximately 200 years later W. Herschel was one of the pioneers to start modelling the structure of our galaxy. These first models were very asymmetric and thus unrealistic when it comes to dynamic evolution (Alfaro, Pérez and Franco 2004).

Time went on, telescopes got bigger until today we look at the sky not only with the bare eye but instead with telescopes sensitive to various wavelengths alongside many kinds of particle detectors. Figure 2.6 shows four different maps - all in galactic coordinates (see appendix C) - obtained through such measurements with decreasing photon energy from left to right and top to bottom. All of them have one thing in common: Sources spread all over the Milky Way dominate by making up the biggest amount of the flux measured. Gamma-rays of energies greater than 1 GeV measured by the Fermi telescope can be seen in the top left image. These are believed to be originating mostly from interactions of cosmic rays with interstellar clouds (Massaro, Thompson and Ferrara 2015). Data received from GAIA made it possible to create a map in the optical range seen in the top right map. Visible light primarily emanate from stars and dark regions within the galactic disc account for dust clouds (Gaia Collaboration et al. 2018). The bottom left picture is made from data by IRAS and shows infrared radiation referring mostly to thermal emission by interstellar dust at around 15 K (Schild et al. 2012). Last but not least at the bottom right one can see a combined map from EBHIS and GASS focusing on the 21 cm line which traces clouds of neutral atomic hydrogen (HI) (HI4PI Collaboration et al. 2016).

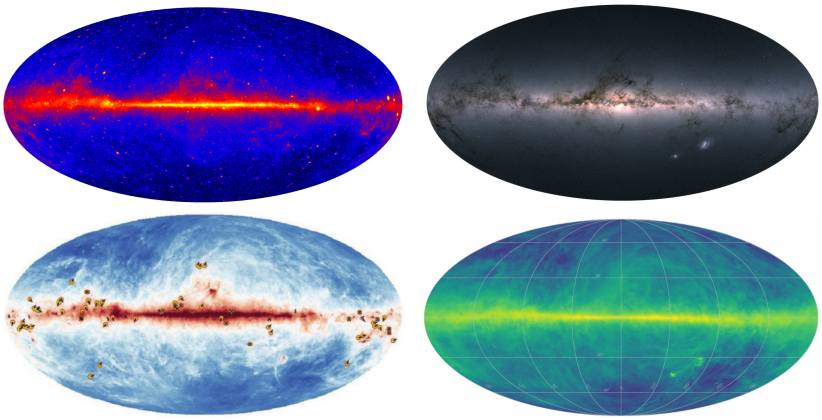

Figure 2.6: *Four all sky maps at different photon energies all in a galactic coordinate system Top left: gamma-ray emission (Fermi telescope, Massaro, Thompson and Ferrara 2015); top right: visible light (GAIA, Gaia Collaboration et al. 2018); bottom left: infrared emission (IRAS, Schild et al. 2012); bottom right:* 21 *cm line (EBHIS and GASS, HI4PI Collaboration et al. 2016)*

These and further measurements got as far as to tell us that the Milky Way is one of around 10^{11} galaxies within the visible universe. Estimations for the number of stars contained in it are of the order of 10^{11} (Unsöld and Baschek 2002) and measurements for it's diameter deliver a value from 46 kpc to 62 kpc. (López-Corredoira et al. 2018) However, measurements like in Clemens 1985 already showed that the interstellar gas of the galactic halo (see figure 2.7 for approximate structure of the Milky Way and its surroundings) mainly resides within a sphere of approximately 16 kpc radius with a mean density of $10^{-2}\,\mathrm{cm}^{-3}$ with big structures of denser material up to $10\,\mathrm{cm}^{-3}$ at average in the bulge can be found (Unsöld and Baschek 2002).

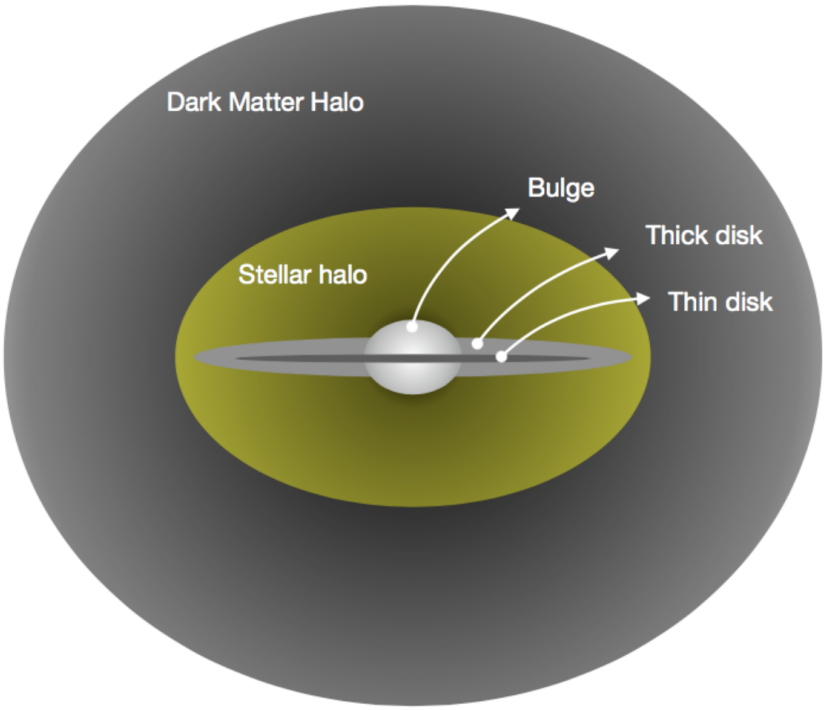

Figure 2.7: *Main structure of spiral galaxies (Granados et al. 2017)*

Hot Bubbles, the Local Bubble and Gould Belt

The average particle density of the galactic disk the sun is located in was found to be around $1\,\mathrm{cm}^{-3}$ mostly made up of molecular and atomic hydrogen. Through HI absorption measurements with light from close by stars it was discovered though, that the Sun resides within a Hot Bubble, the Local Bubble or Local Cavity with a particle density a hundred times smaller but at temperatures of around $10^6\,\mathrm{K}$ (Unsöld and Baschek 2002).

Furthermore, it seems the Local Bubble by far is not the only one of that kind but instead this phenomenon is quite common. They are believed to be formed by massive stars partly through the huge amounts of stellar wind they produce[3] as well as the supernovae they end in when they run out of matter to fuel the fusion processes inside of them. Winds and supernovae from big stars already within of such bubbles reheat their interior and shape the walls. The Local Bubble is believed to have formed from 17 supernovae of stars between $8\,\mathrm{M}_\odot$ (solar masses) and $22\,\mathrm{M}_\odot$ (Reis et al. 2011).

Through X-ray measurements it was possible to locate the walls of the Local Bubble. The shape found can be seen in figure 2.9 in the form of cuts at different angles, the Sun always is the centre of the coordinate systems. As can be seen the Sun is between 50 pc and 200 pc (depending on direction) away from the Bubble's walls (cf. Liu et al. 2017, Lallement et al. 2014). The Gould Belt seems to account for a big part of the Local Bubble's boundaries. This belt is a ring of unknown origin that contains several OB associations and is tilted towards the galactic plain by about 20°. Figure 2.8 shows a schematic of its structure (Lallement 2009).

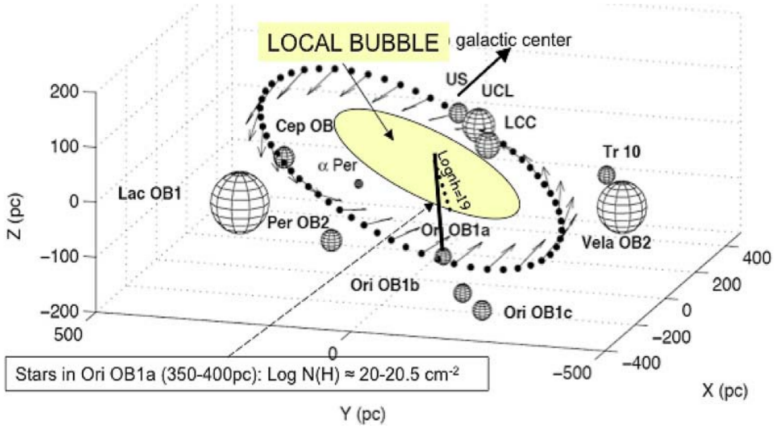

Figure 2.8: *Schematic view of the Gould Belt (Lallement 2009)*

Through hydrodynamic simulations concerning the formation of the Local Bubble over time the thickness of its wall now is estimated to be between 2 pc and 5 pc and its density around $10^2\,\mathrm{cm}^{-3}$ to $10^3\,\mathrm{cm}^{-3}$ (Reis et al. 2011; Krause et al. 2014b; Krause et al. 2014a).

[3] The more massive a star is when fusion reactions start in it, the higher the percentage of his total mass is lost through winds over its life (Smith 2014). For example a $25\,\mathrm{M}_\odot$ star through winds has an output of about $5\,\mathrm{M}_\odot$ before the SN explosion (Diehl 2013).

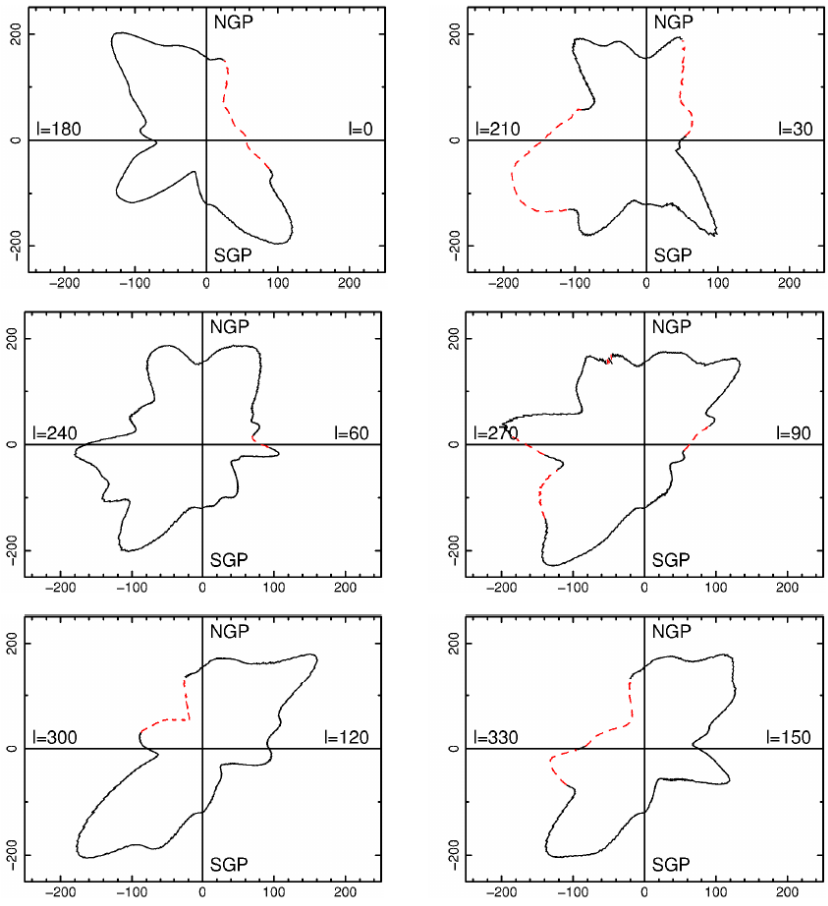

Figure 2.9: *The radius of the LHB in great-circle cuts through the Galactic poles along the labelled longitude. The red dashed line corresponds to directions of non-LHB bright extended sources (Liu et al. 2017)*

Local Fluff and Local Cloudlets

The Sun within the Local Bubble is located in a cloud called the Local Fluff or Local Interstellar Cloud, which has a higher density than the LB interior of $10^{-1}\,\mathrm{cm}^{-3}$ and a size of approximately 10 pc in diameter. It is one of a group of six clouds that are believed to have formed before the bubble and altogether they are called the Local Cloudlets, all of similar sizes. They mainly are made up of warm gas at 800 K (Lallement et al. 1998; Unsöld and Baschek 2002).

Interplanetary Medium

The volume closest to us that we are interested in is the interplanetary medium with a diameter of approximately 70 AU which equals 0.3 mpc. The density is highly variable. Near earth it is between $5\mathrm{cm}^{-3}$ and $10^2\mathrm{cm}^{-3}$ and roughly follows a $1/R^2$ law where R is the distance to Sun (Nieto and Turyshev 2004; Nieto, Turyshev and Anderson 2005).

As a comparison to all the numbers mentioned, the particle density of the atmosphere at sea level here on earth is around $10^{19}\,\mathrm{cm}^{-3}$ while at distances of 50 km to 100 km from the earth surface this already decreases by a factor of approximately 1000 (Andrews 2010). However, if one wants to compare the atmosphere to the interstellar medium one also needs to take in account, that unlike the interstellar clouds the atmosphere is not made up of hydrogen atoms but mostly heavier atoms like nitrogen.

2.3.2 Intergalactic Medium

How densities change when leaving the Milky Way is hard to answer. In absence of a sufficient amount of stars for doing absorption measurements like they can be done in the Milky Way, one uses hydrodynamic models that predict a warm-hot intergalactic medium (WHIM), a plasma with temperatures from 10^5 K to 10^7 K and densities between 10^{-6}cm^{-3} and $10^{-5}\,\text{cm}^{-3}$. (Majumdar, Bharadwaj and Choudhury 2012) Embedded in this intergalactic medium there are 10^{-2} galaxies per cubic megaparsec (McQuinn 2016).

Active Galactic Nuclei

However, there is one kind of galaxies that is special to what we are interested in for this study - ones with an AGN. This term refers to a supermassive black hole of millions to billions of solar masses at their centre. What makes them that special is that they are believed to be one of the strongest galactic particle accelerators and for example at least carrying part of the responsibility for the cosmic ray spectrum at Ankle energies and above. Particles accelerated through active galactic nuclei are emitted in jets perpendicular to the accretion disc. If this jet points towards earth the AGN is called a Blazar (Unsöld and Baschek 2002).

As can be seen in figure 2.10 AGNs are isotropically distributed all over the sky[4]. FSRQ (Flat Spectrum Radio Quasars), BL Lac obj. (BL Lacertae ojects), AGN unk. type (AGN unknown type) and radio galaxies in this figure represent different types of AGN. One of the closest ones is at the centre of the galaxy Centaurus A at a distance of 3.8 Mpc (Harris 2010).

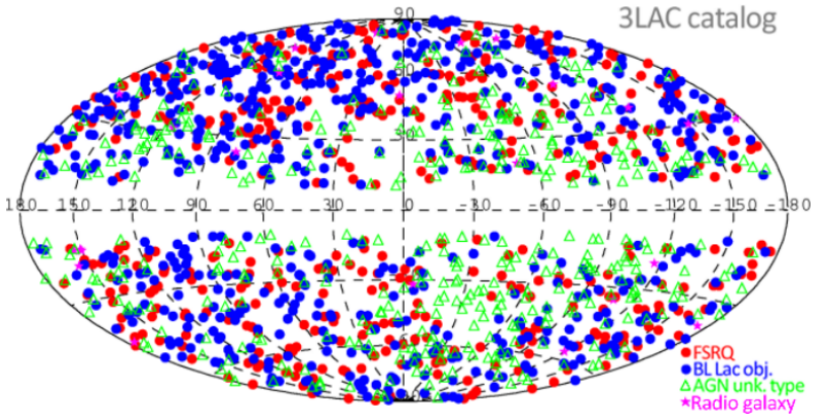

Figure 2.10: *Distribution of active galactic nuclei galaxies detected by the Fermi satellite (Britto et al. 2016)*

[4]The Milky Way cover part of it though, which is why no AGN are seen at galactic latitudes of around 0°.

3

Cosmic Ray, Neutrino and Gamma Measurements

In order to properly interpret models that are based on actual data it is inevitable to know about the experiments behind it - where they were made, how and what are limiting aspects on the results.

This chapter's first section will focus on general ways how to measure the three cosmic messengers compared during this thesis while giving exemplary experiments working accordingly. Most characteristics have been determined through using different approaches and finding a best-fitting model for the combination. These, and what influence this has on the outcome of this thesis will be discussed in chapter 5.

As this thesis is focussed on neutrino data interpretations, the IceCube observatory will then be outlined in more detail than the other experiments in the second section.

3.1 Measurement Experiments

3.1.1 Particle Detectors

When high energetic particles interact with matter they can either lose energy through ionisation of atoms, interaction with nuclei or emission of radiation. The outcome of these processes can be measured and form the basic principles of particle detectors. Besides flux directional information also is a crucial component of measurement but unfortunately it is neither possible to track high energy photons nor neutrinos themselves. However, one can track secondary particles emerging from interactions which in total carry the same momentum as the primary particles and thus can be used to reconstruct the track. Hence particle detectors are used for detection of all three of our relevant messengers (Unsöld and Baschek 2002).

One of the oldest detector types are bubble chambers. Ions emerging along the track of the incoming particle function as condensation nuclei in a superheated liquid leaving a track in it. The thickness of the visible track then is proportional to the passing particle's energy. Applying an additional magnetic field makes it possible to determine the charge via the track's curvature (Unsöld and Baschek 2002).

Making the track visible permanently can be accomplished by using plastic detectors or AgBr crystals. Both detector types change their chemical composition and after development leave an image of the passing particles similar to a photograph (Unsöld and Baschek 2002).

The transformation into an optical signal can be achieved through scintillator crystals or using the effect of Cherenkov radiation. Ionizing beams passing through scintillators excite atoms within, that then through emission of light deexcite into their ground state. Cherenkov light occurs when a charged particle passes through a material with a velocity higher than the speed of light in this material. Around the particle a cone of light appears with an opening angle proportional to the particle speed (Klapdor-Kleingrothaus and Zuber 1997). The optical signals then also need to be processed, which often is done using photomultipliers. These are devices that

utilize the photoelectric effect of low energy photons (order of eV) and with a cascade principle then amplify the current up to more than a million times (Unsöld and Baschek 2002).

Charged particles can be detected using a thin gas with a high voltage applied. A particle passing through such a Geiger-Mueller counter will ionize the gas and give a short current pulse that can be detected. Building an array of such detectors creates a spark chamber, which also is sensitive to direction of the particles (Longair 1992).

Finally one can also use solid state detectors made of very pure semiconductor crystals, usually silicon or germanium. They function similar to Geiger-Mueller counter, but instead of ionization, electron-hole pairs are created that with an applied voltage result in a current. Their advantage over Geiger-Mueller detectors is their very good energy resolution through the very precise energy dependence for created electron-hole pairs (Unsöld and Baschek 2002).

Since each of the detector types above is better for measuring different characteristics. Usually a combination is used in order to gain as much information about events as possible.

3.1.2 Cosmic Rays

For cosmic rays there are two big types of measuring a spectrum. One can either examine the primary particles or secondaries that emerge through interaction with matter. While detecting primary particles is favourable, for one is able to not only determine the energy of the particle but also its charge and thus the type of nucleus, this only is possible for particles below 100 TeV. Beyond these energies the occurring fluxes are too low to still be measured directly (Klapdor-Kleingrothaus and Zuber 1997).

Direct measurements are based on directly detecting the interaction of a cosmic ray particle with matter. Atmospheric absorption of cosmic rays is the first challenge to overcome. Hence all experiments for direct measurements are airborne, either on balloons, that go into the outer layers of the atmosphere, or spacecraft.

The Japanese-American Collaborative Emulsion Experiment (JACEE) experiments were examples for balloon carried ones between 1979 and 1996. Charge, direction and energy were being observed for nuclei between 1 TeV and 100 TeV using plastic emulsion plates and lead calorimeters (JACEE Collaboration 1997).

An experiment performed in space was the Chicago Egg carried on the Challenger Space Shuttle in 1985. Cosmic rays in an energy range from 40 GeV/Nucleon to several TeV/Nucleon were investigated through a Cherenkov detector paired with two scintillators (L'Heureux et al. 1990).

However, the higher the particle energy one wants to observe, the lower the fluxes are. In order to still being able to get results one would need bigger and bigger detectors, which at one point leads to being unaffordable. Indirect measurements on the other hand detect secondary products and particle cascades from interactions of high energetic cosmic rays with our atmosphere or even sufficiently long lived particles (mostly muons) with detectors placed on the ground (Klapdor-Kleingrothaus and Zuber 1997). These detectors usually rely on either fluorescence happening in air or Cherenkov radiation emitted in air or water tanks on the earth surface.

The Pierre Auger Observatory in Argentina is sensitive to cosmic rays between 100 PeV and 1 ZeV and has been detecting Cherenkov light and luminescence as well as a radio signals in the atmosphere with detectors spread over 3000 km^2 since 2004 (Unger and Pierre Auger Collaboration 2017).

Working in close collaboration with the Auger group Akeno Giant Air Shower Array (AGASA) experiment in Japan collects data in a very similar way, using scintillation detectors on the surface and muon detectors spread over 100 km^2. It has been operating since 1989 (Takeda et al. 1999).

3.1.3 Gamma-Rays

Similar to that of cosmic rays, gamma-ray observers suffer from both, the problem of high atmospheric absorption and that of very low fluxes in high energy. Both challenges are solved the same way as for cosmic rays: The lower energy part (100 keV to up to around 300 GeV) is being observed with instruments on balloons and spacecraft while for the very high energy part (typically above 100 GeV) ground based observatories are in use.

The International Gamma-Ray Astrophysics Laboratory (INTEGRAL) is a satellite launched in 2002. Its two main instruments both are sensitive to gamma-rays from 15 keV to 8 MeV. Both are solid state detectors with masks in order to do source tracking through shadowing of specific detector segments depending on incident angle (Diehl 2013).

The Fermi Gamma-Ray Space Telescope was launched in 2008 and includes two instruments on-board. The Large Area Telescope (LAT) is based on detecting pair production of electrons and positrons and through this determine the energy and trajectory of the gamma-rays in the range of 20 MeV to 300 GeV. An all sky detector for gamma-ray bursts is provided by the Gamma-Ray Burst Monitor (GBM) as a combination of different scintillator crystals for being an effective measuring device between 8 keV and 40 MeV (Atwood et al. 2009; Meegan et al. 2009).

Figure 3.1: *Picture of the two MAGIC telescopes located at La Palma (Spanish National Research Council 2017)*

Based on detecting Cherenkov light from air showers produced by high energetic gamma-rays the Major Atmospheric Gamma Imaging Cherenkov Telescope (MAGIC) started its observation with one telescope in 2004. Since 2008 it has been using two 17 m diameter parabolic telescopes in order to detect photons reaching from 25 GeV to 30 TeV (Moralejo 2009, Dazzi et al. 2015). An image of the two parabolic Cherenkov telescopes can be seen in figure 3.1.

Most common detector types are sensitive to each of our three astronomic messengers. This both is a problem and an opportunity. Naturally, if one wants to examine one of the three, the others create noise and have to be filtered out. However, being able to distinguish between the

types makes it possible to use one detector for more than just one purpose. MAGIC for example both is used to study cosmic rays and gamma-rays.

3.1.4 Neutrinos

I have done a terrible thing: I have postulated a particle that cannot be detected.
– Wolfgang Pauli

With cross sections being by approximately ten orders of magnitude smaller than that of protons for example, neutrino detectors have to be sufficiently big and thus all of them are ground-based. Since they only interact weakly though, their reactions with matter is very limited, which opens the possibility of one kind of measurement that wouldn't be possible in such a way for other particles: chemical prove of neutrino interactions. A very famous experiment utilizing this in the 1960s has already been mentioned, the one Davis, Harmer and Hoffman 1968 used in order to prove the existence of solar neutrinos and to very precisely determine the total number of neutrinos interacting. They placed a $380\,\mathrm{m}^3$ tank of perchloroethylene in a goldmine in Lead, South Dakota, where via the interaction

$$\nu_\mathrm{e} + {}^{37}\mathrm{Cl} \rightarrow {}^{37}\mathrm{Ar} + \mathrm{e}^-$$

the radioisotope ^{37}Ar could be extracted by bubbling helium through the tank and counted measuring the decay rate.

However, this kind of experiments carries no direction information at all, which makes Cherenkov or scintillator experiments more suited in order to build telescopes, as are interesting for this thesis. The Super-Kamika Neutrino Detection Experiment (Super-Kamiokande), successor of the similar but smaller Kamiokande Observatory, has started it's work in 1996. It uses photomultipliers to detect Cherenkov light emitted in a tank of ultra pure water. This experiment finds its most important field in measuring the solar neutrino flux and neutrino oscillations (Klapdor-Kleingrothaus and Zuber 1997).

One thing that is problematic about experiments like Super-Kamiokande, using a water tank, is that they are limited in size and storing the needed amount of water for a big enough detector to detect low fluxes one again finds at high energies is difficult. Hence some groups started using big natural reservoirs of pure water - liquid as well as frozen - and putting photomultiplier devices in. An example for this is the Antarctic Muon And Neutrino Detector Array (AMANDA). As predecessor and now part of IceCube, AMANDA used the same principle, detecting Cherenkov light of secondaries in ice. It was in operation from 1996 on until it became part of IceCube, that was built in steps from 2005 to 2010. (cf. section 3.2; Andres et al. 2000; Aartsen et al. 2017c).

3.2 IceCube

Located on an Antarctic glacier the IceCube Neutrino Observatory is one of the largest experiments on earth. In figure 3.2 one can see its general set-up and tremendous size and as a comparison that of the Eiffel Tower. The following gives an overview of different researches done with it and a more detail on the measurement of the data this thesis focuses on. Fundamental to this whole chapter is the book by Aartsen et al. 2017c.

3.2.1 How to do Physics with an Ice Cube

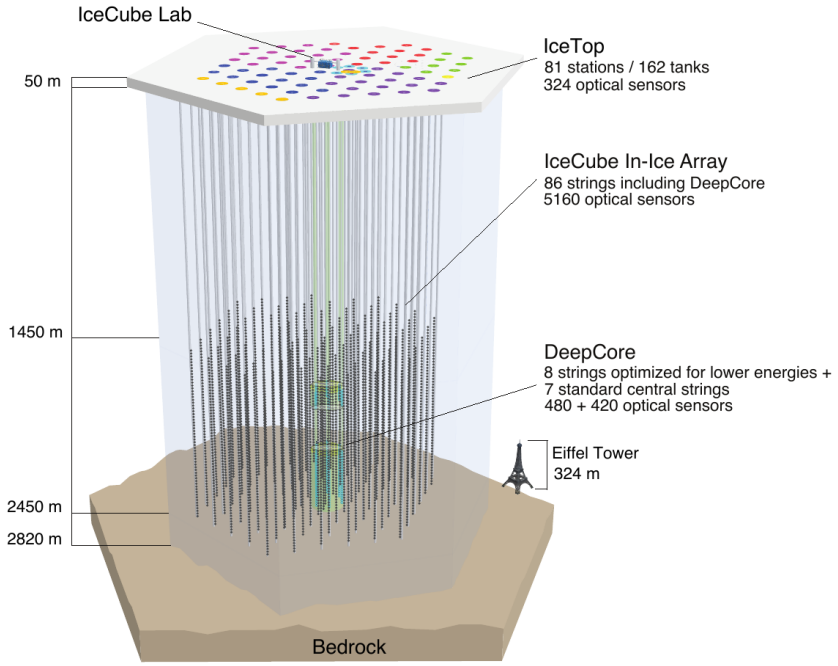

Figure 3.2: *The IceCube Neutrino Observatory with the in-ice array, its sub-array DeepCore and the cosmic ray air shower array IceTop. The different string/station colours represent the deployment seasons (Aartsen et al. 2017c).*

With about three kilometres of thickness the very pure ice cap at the IceCube site provides the necessary amount of interaction material for neutrinos while also being sufficiently transparent to the Cherenkov light. The whole observatory uses similar single detectors called digital optical modules (DOMs) that consist of a photomultiplier and on-board logic in glass spheres to withstand the high pressures.

IceCube In-Ice

IceCube In-Ice Array, the main part of the whole observatory, is made up by 78 strings with 60 DOMs each (which makes a total of 4680 DOMs). The vertical separation of the DOMs is 17 m and the strings are arranged in a hexagonal footprint with 125 m distance between each two neighbouring strings. Even though all photomultipliers point downwards they can detect Cherenkov light from any direction due to dispersion effects in the ice. Two classes of events define how neutrinos are being measured - track-like and shower-like. The track-like events originate from muons being produced by charged current interactions of muon neutrinos. Due to the muons travelling very far before vanishing again in interactions an angular resolution of approximately 0.6° can be acquired. However, since the track usually ends outside the detection area of IceCube (and/or starts outside) they do not deposit their whole energy within the experiment. Thus the neutrino energy resolution in this kind of events is bad. The second kind of events, shower-like, are electrons or taus that very fast end in an electromagnetic or hadronic shower. Since they deposit their whole energy within the detector this can be measured more precisely, but the more spherical shape defines the angular resolution only to a range between 10° and 30°. This setup makes IceCube most sensitive to neutrino energies between 100 GeV and 1 ZeV.

DeepCore

Additional eight strings with partly more dense DOM spacing together with seven strings of the In-Ice set-up form the DeepCore, which is made for lower energy neutrinos. Different to the remaining array, that has an energy threshold of 100 GeV in DeepCore neutrinos down to 10 GeV can be measured in order to detect for example atmospheric neutrino oscillations or neutrinos from Galactic supernovae.

IceTop

Together with some parts of the outer layer of the In-Ice array the IceTop works both as an anti-coincidence unit and to measure cosmic rays. Cosmic rays interacting with the atmosphere give rise to muons that can penetrate IceCube. In order to not falsely interpret these as neutrinos, events with a time correlation with muons entering IceCube from the outside are being filtered out of neutrino measurements while at the same time providing data for cosmic rays. IceTop consists of 162 ice-filled tanks each with 2 DOMs in it and is sensitive to primary cosmic rays in the PeV and EeV range, thus fully covering both the Knee and the Ankle (cf. 2.2).

3.2.2 Science Topics with IceCube

Not only can IceCube be used to pursue neutrino astronomy, there are several other topics which the detectors can be utilized for. Two additional areas are cosmic rays and neutrino physics apart from cosmology. IceCube examines cosmic rays by measuring particles emerging from interactions with our atmosphere. Through the knowledge about cosmic rays it is also possible to provide neutrino oscillation data to add up to that provided by Super-Kamiokande and further experiments such as MINOS or T2K.

Relying on the Antarctic glacier as a detector makes it favourable to study its behaviour such as movement of the glacier ice or pressure dependence of diffraction in ice as well.

Also, IceCube provides data to observe dark matter through studying specifics of neutrino flux from different regions like the Sun, the galactic halo, galaxy clusters or the Earth.

4

Multi-Messenger Approaches

The first section of this chapter will focus on the data retrieved from IceCube. A recap of the analysis done by IceCube concerning isotropy and spectrum will be followed by a description of how I determined these characteristics and what the results were. This way both, a second view on the data through different algorithms and a basis for discussion in chapter 5 about the theoretical fluxes obtained with cosmic ray data, are provided.

Section 4.2 then explains how the initial cosmic ray flux is used to predict a neutrino and a photon spectrum. After summarizing the assumptions made, the focus will be on examining two aspects of the spectrum namely what fraction of neutrinos can be expected from what distance and how changing the composition of cosmic rays affects the resulting spectrum. Finally two more important aspects will be discussed: How the spectrum will be composited of the different neutrino flavours with interactions at various distances considering neutrino oscillations and what a gamma-ray flux accompanying these neutrinos would look like.

4.1 IceCube Data Analysis

The experiment data used is that released on 21st October 2015 by IceCube Collaboration 2015 concerning their observation of ultra high energetic neutrinos above 10 TeV between 2010 and 2014. Analysis of isotropy and spectrum of a part of this data have been done in Aartsen et al. 2014. Due to the fact that it had been released earlier, it only makes use of the first three years (37 of a total of 54 events). Events 28 and 32 are excluded from calculations in the paper and will also be within this thesis for they are reported to most likely be coincidental events from air showers. Characteristics of the latter are not even specified in the data release.

4.1.1 Previous Analysis by IceCube

The neutrino data are characterized by their deposited energies in the detector between 10 TeV and 2 PeV, their direction of incident, the event type (shower or track) and the time of incident (in Modified Julian Date). The energy and incident angle both come with uncertainties.

Figure 4.1 shows a sky map of neutrino events detected in IceCube over four years as a Hammer-Aitoff projection in galactic coordinates. Event number and type are given for each event. Shower like events marked with red + (mean angular resolution 15°), muon track events marked with black x (mean angular resolution 1°). The green curve shows the equator line with all events above it coming from the northern hemisphere, all below from the southern.

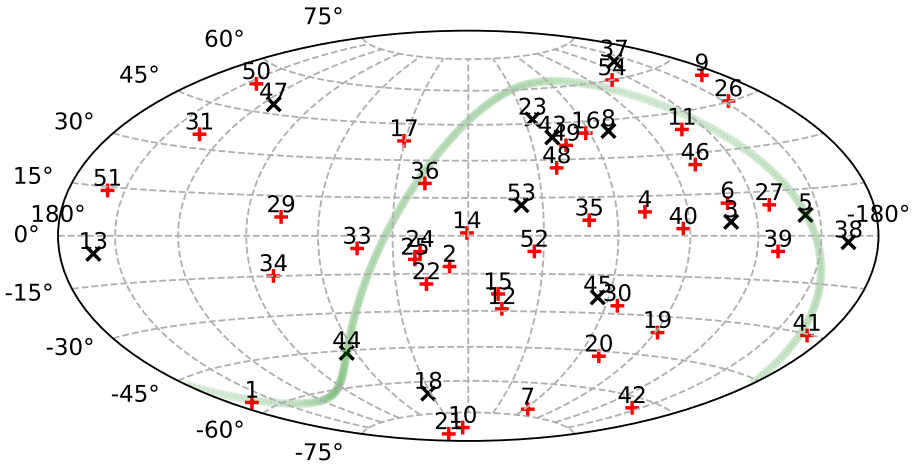

Figure 4.1: *All Sky Map of Neutrinos > 10 TeV detected by IceCube over four years*

Aartsen et al. 2014 estimates that the flux is isotropic by counting events within certain declination bins above various threshold energies. Figure 4.2 shows this for an energy threshold of 60 TeV.

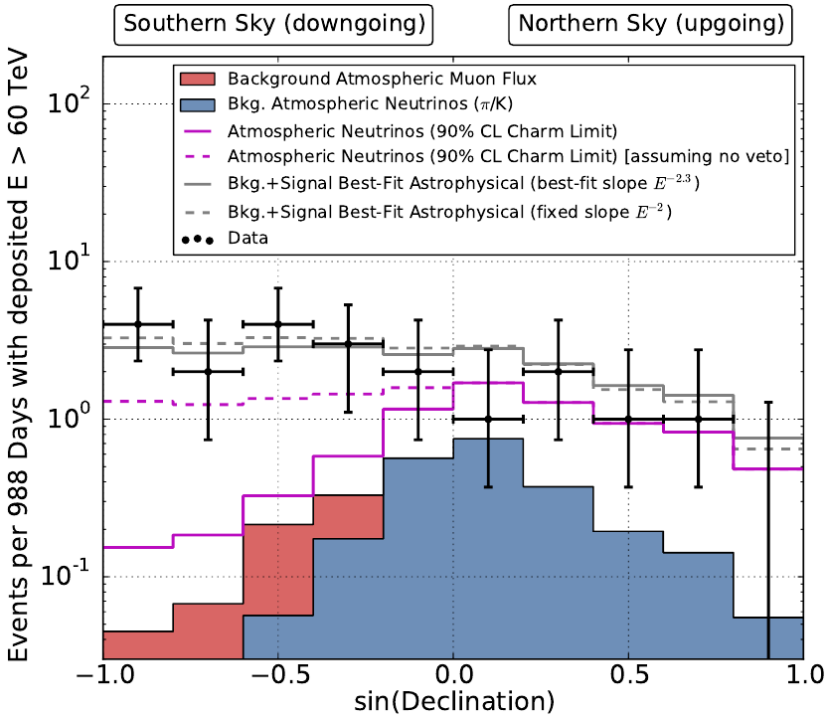

Figure 4.2: *Comparison of zenith distribution of detected neutrinos with expected atmospheric fluxes before and after removal of events accompanied into the detector by muons from the neutrinos' parent air shower (Aartsen et al. 2014)*

The flux $\phi(E) = {}^{\mathrm{d}N}/_{\mathrm{d}E}$ has been analysed by Aartsen et al. 2014 both as a broken power law with spectral index -2 and with an unbroken power law ansatz with $E^2\phi(E) = 1.5 \cdot 10^{-8}({}^{E}/_{100\,\mathrm{TeV}})^{-0.3}\,\mathrm{GeV\,cm^{-2}\,s^{-1}\,sr^{-1}}$ as a best fit. Figure 4.3 shows into which bins the incoming events were separated for the broken power law as well as the result after subtracting the number of events expected from atmospheric neutrinos.

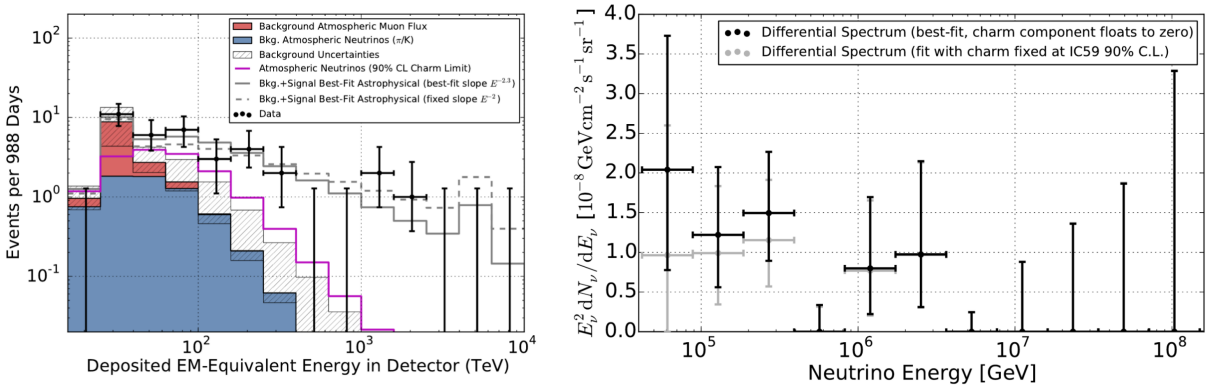

Figure 4.3: *Left: binned counts per energy in comparison to expected atmospheric neutrino counts*
Right: piecewise binned flux of non-atmospheric neutrinos
(both from Aartsen et al. 2014)

4.1.2 Spectral Analysis

In this thesis, two different likelihood functions, a Gaussian and a Poissonian, are used to determine the spectral shape of the neutrino flux, and to compare the resulting parameters and uncertainties.

In figure 4.4 the counts per energy bin can be found. Horizontal error bars refer to the size of each bin, vertical ones to estimated counting uncertainties for random Poisson variables. As an estimate of the uncertainties, the square root of the number of counts in each bin, is used. If the counts are zero, the estimate for the uncertainty is $\sqrt{52/14}$ which divides the number of all events by the number of bins. The orange bars indicate the number of counts a continuous power law flux, fitted using Poissonian likelihood, would predict. How this was done will be explained later on in this section.

As shown in appendix A.1, the Poisson likelihood circumvents the issue of estimating uncertainties, as no uncertainty for the number of counts has to be defined.

Bins were defined by a constant logarithmic size from $10^{1.2}$ TeV up to 10^4 TeV ($10^{1.2}$ TeV - $10^{1.4}$ TeV,...,$10^{3.8}$ TeV - $10^{4.0}$ TeV).

As relation between counts and flux, a function in its basic version given by equation 4.1 (from IceCube Collaboration 2013) is used. A_{eff} refers to the energy dependent effective area of IceCube in m^2, ϕ_ν to the flux in $\mathrm{eV}^{-1}\,\mathrm{m}^{-1}\,\mathrm{s}^{-1}\,\mathrm{sr}^{-1}$ and t_{obs} to the total time over which the events were being detected in s. The factor 4π occurs due to counts being integrated over all directions.

$$\phi_\nu = \frac{\mathrm{d}N}{\mathrm{d}E_\nu \cdot 4\pi \cdot A_{\mathrm{eff}} \cdot t_{\mathrm{obs}}} \tag{4.1}$$

The effective area A_{eff} as a function of energy can be seen in figure 4.5. The peak for $\bar{\nu}_{\mathrm{e}}$ at 6.3 PeV is caused by resonant W production with atomic electrons which is only relevant for electron antineutrinos due to number densities of charged leptons other than electrons in matter is negligible. Plotted is the effective area of the IceCube detector for the three flavours. The given version still is a simplified one of the actual effective area for the value would also depend on incident angle.

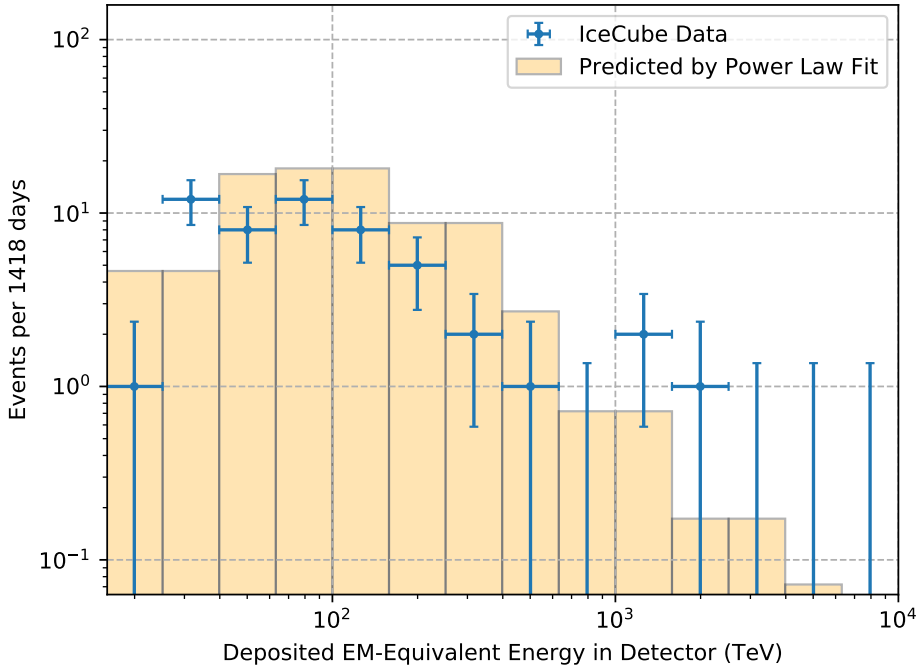

Figure 4.4: *Counts per energy bin as a function of energy deposited in detector compared to counts predicted by power law fit*

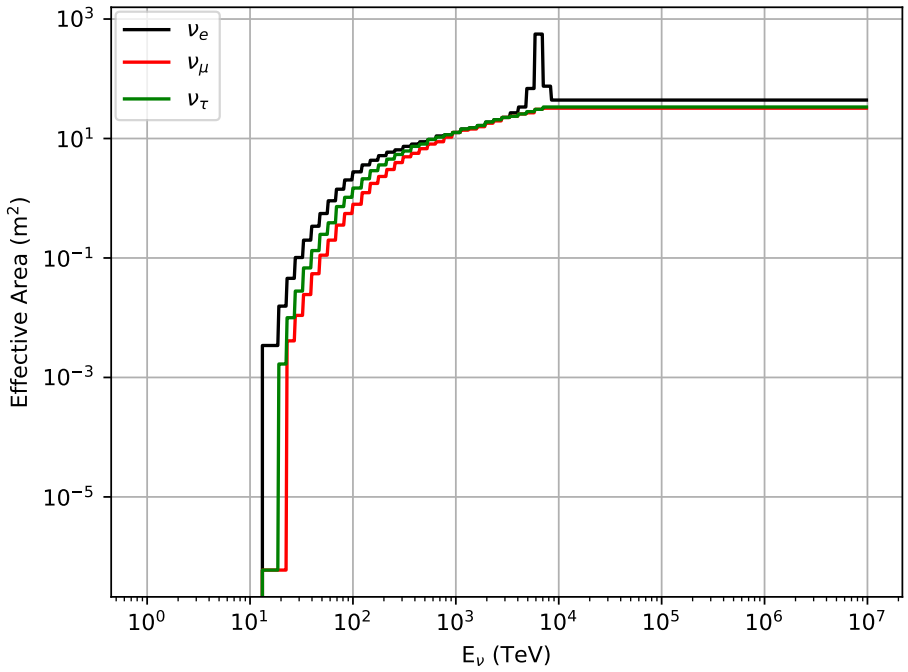

Figure 4.5: *Effective area of the IceCube detector for neutrino events of the three flavours averaged over all incident angles and with an equal flux for neutrinos and antineutrinos assumed (IceCube Collaboration 2013)*

Having different effective areas for the three flavours makes the calculation more difficult though for one would have to use the flavour specific value for each event. However, the only way to distinguish between the flavours from the data provided by IceCube is the event type and also only one distinction works - tracks are most certainly all caused by muon neutrinos[1]. Due to this when calculating the total neutrino flux track like events will be treated as muon neutrinos and other events as an equal mixture of electron and tau flavoured ones with the effective area calculated as the harmonic mean of those two as

$$A_{\text{eff, total}} = \left(\frac{A_{\text{eff},\tau}^{-1} + A_{\text{eff, e}}^{-1}}{2} \right)^{-1},$$

which is motivated by the effective area appearing as a denominator in the relevant function 4.1.

This is now used to get two different estimates on the spectrum(see appendix A.1 for details on the fit). All estimated fluxes represent the sum over all flavours and both neutrinos and antineutrinos.

A first order estimate for the flux was obtained for each bin by assuming a constant flux in each bin. This way the flux in each bin is given by

$$\phi_\nu = \frac{N_{\text{bin},\mu}}{\Delta E_{\text{bin}} \cdot 4\pi \cdot A_{\text{eff},\mu} \cdot t_{\text{obs}}} + \frac{N_{\text{bin}} - N_{\text{bin},\mu}}{\Delta E_{\text{bin}} \cdot 4\pi \cdot A_{\text{eff,total}} \cdot t_{\text{obs}}},$$

where N_{bin} and $N_{\text{bin},\mu}$ are the total number and the number of track-like events in a bin respectively and ΔE is the energy range of a bin. While Gaussian likelihood delivers symmetric boundaries of uncertainties, Poissonian does not. Figures 4.7 and 4.6 show the two results respectively. Both are scaled to the same units as used in the analysis by IceCube for comparison. Uncertainties calculated using a Gaussian likelihood at high energies are cut of in order to being able to see the interesting part and because the only reason for them being that big at high energies is the E^2 factor. The highest of these uncertainties reaches a value of approximately 50 in this plot.

For the second spectral analysis a continuous power law according to $E^2\phi(E) = a(E/100\,\text{TeV})^\beta\,\text{GeV}\,\text{cm}^{-2}\,\text{s}^{-1}\,\text{sr}^{-1}$ was used where a and β were the two fitting parameters. As function to be fitted to the counts as seen in figure 4.4, for each bin the integral of the flux over the according energy range multiplied by $4\pi \cdot A_{\text{eff,total}} \cdot t_{\text{obs}}$ was used. For this ansatz no distinction between track-like and shower-like events was made, thus the total effective area is the harmonic mean over all three flavours. Using a Poisson likelihood one receives $a = (3.0 \pm 1.0) \cdot 10^{-6}$ and $\beta = -1.37^{+0.25}_{-0.24}$, with the Gaussian one $(2.7 \pm 0.4) \cdot 10^{-6}$ and -1.43 ± 0.21 as a and β respectively are the best fitting parameters. In figure 4.4 the counts one would expect with the Poissonian fit in each bin are compared to the IceCube data.

[1] Xu and IceCube Collaboration 2017 and Aartsen et al. 2014 state, they are only caused this way but still there is a very small chance for a tau neutrino becoming a tau that decays into a muon before interacting with matter.

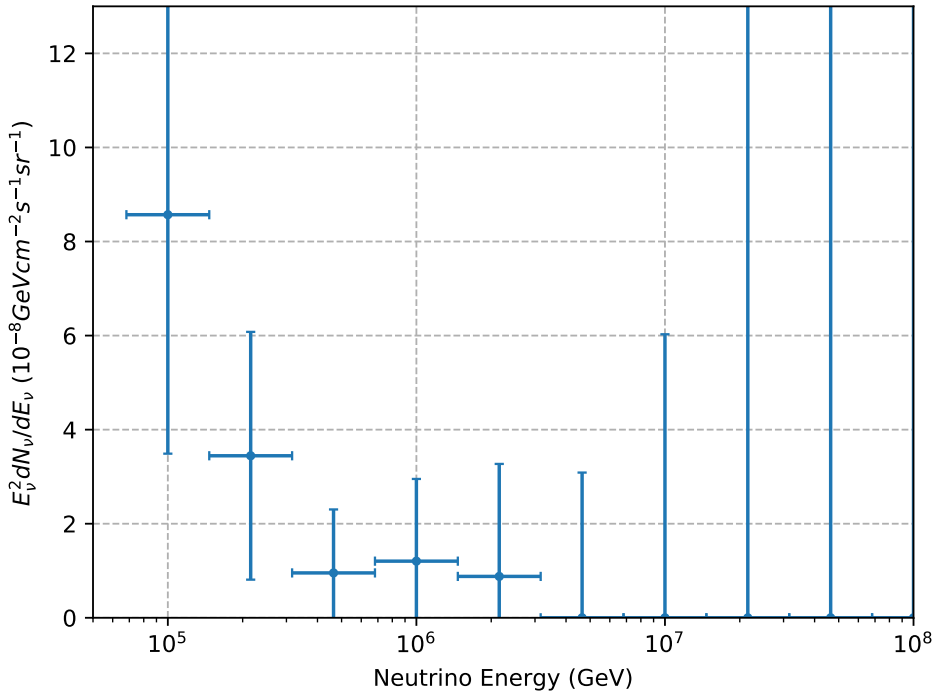

Figure 4.6: *Zero Order Flux Estimate for Neutrino Counts* > 10 *TeV with Gaussian Uncertainties*

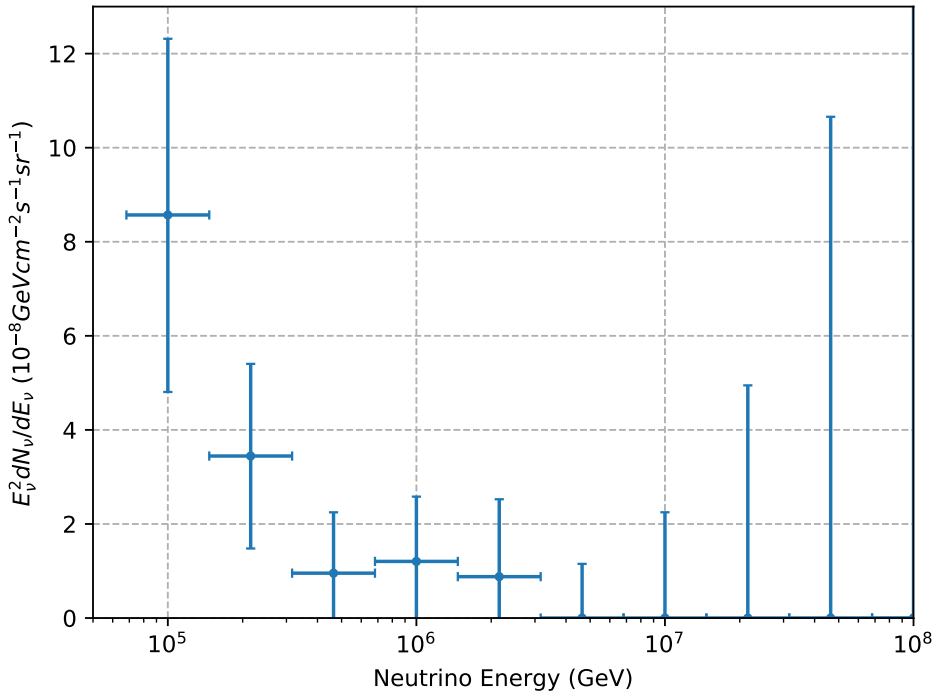

Figure 4.7: *Zero Order Flux Estimate for Neutrino Counts* > 10 *TeV with Poissonian Uncertainties*

4.1.3 Spatial Analysis

The analysis in Aartsen et al. 2014 on the spatial distribution of neutrinos only investigates isotropy in one direction, with increasing declination of events. In this thesis the analysis is done on a way similar to how the CMB was analysed using data from the Wilkinson Microwave Anisotropy Probe (WMAP) spacecraft. The principle of this analysis is to find out, whether variations from a homogeneous flux appear in a certain pattern by expanding the flux as a linear combination of spherical harmonics. Or rather, since there are no defined axes important to us, the analysis is done by expanding the correlation function of each two points on the sphere as a combination of Legendre polynomials (cf. appendix A.2). This section focuses on how one can process the data using them (Bennett et al. 2003).

To avoid the low number statistics and at the same time to take the uncertainties of the neutrino localisations into account, an auxiliary variable is defined: This pseudo flux is calculated for each point of a raster 1° times 1° as a sum over all events. For each event and pixel the value is gained by dividing the pixel size by the event specific effective area and the total duration of the experiment and multiplying this value by a Gaussian factor representing the ratio between the angular separation between event and pixel and the uncertainty in direction given for the event in the data. The resulting number is normalised such, that integrating the pseudo-flux for event over the whole sky gives $1/A_{\mathrm{eff}} t_{\mathrm{obs}}$.

For an expansion into Legendre Polynomials only the variation form the mean $\phi_{\mathrm{p,\,mean}}$ is of interest, for which reason the mean of the fluxintegrated map was subtracted, leading to a difference map.

The next step was to extract a correlation function of cosine theta $f(\cos\theta)$ from this which is expanded in Legendre polynomials P_l with scaling parameters C_l. Equation 4.2 shows how $f(\cos\theta)$ is defined: It is the mean value of the products of $\Delta\phi_{\mathrm{p}}$ of each two points in the sky specified by unit vectors $\boldsymbol{m}$ and $\boldsymbol{n}$ with $\boldsymbol{m} \cdot \boldsymbol{n} = \cos\theta$. C_l then provide information on how strong which multipole can be seen in the sky in such a way, that when one specific C_{n} is much larger than all others the predominant feature appearing in the flux is one with a typical angular separation between minimum and maximum value of this flux of $180°/n$ (called an n-pole; Bennett et al. 2003).

$$f(\cos\theta) = \left\langle \frac{\Delta\phi_{\mathrm{p}}(\boldsymbol{m})}{\phi_{\mathrm{p,\,mean}}} \frac{\Delta\phi_{\mathrm{p}}(\boldsymbol{n})}{\phi_{\mathrm{p,\,mean}}} \right\rangle = \sum_l \frac{2l+1}{4\pi} C_l P_l(\cos\theta) \tag{4.2}$$

A sample with a very high number of events, where randomly appearing patterns don't play a role any more, will with these C_l very precisely show what patterns occur in the data. Perfect isotropically distributed neutrinos would then cause all C_ls to be approximately 0. However, since with a low number of events there is a bigger possibility of a pattern to occur at random than with big numbers of events. To estimate the quality of such an analysis with only 52 neutrinos, we simulate data sets from perfect multipoles with this number. Here, multipoles with $n = 0, 1$ and 2, according to isotropic, dipole and quadrupole flux, were generated. In order to produce all samples the events from the original data were used for all values except the exact direction. Directions then first were sampled as hard multipoles according to their spatial uncertainties as given by IceCube measurements. Here we generate 100 samples each to generate data sets as defined by the following:

1. Isotropic ($n = 0$): event randomly placed anywhere on the sky, meaning the right ascension being between 0° and 360° and the declination between −90° and 90°

2. Dipole ($n = 1$): event placed in the northern hemisphere, meaning the declination is strictly positive

3. Quadrupole ($n = 2$): event placed such that either right ascension is within 0° and 180° and the declination is positive or the right ascension between 180° and 360° and the declination negative

With these rules 100 samples for each of the three cases were generated to find the mean value and standard deviation of each C_l and n respectively. Figure 4.8 shows a comparison of this statistical analysis together with the measured IceCube neutrino analysis. For the three simulated cases, the drawn lines and the shaded areas correspond to the mean values and the $1\,\sigma$ regions calculated from the 100 samples respectively.

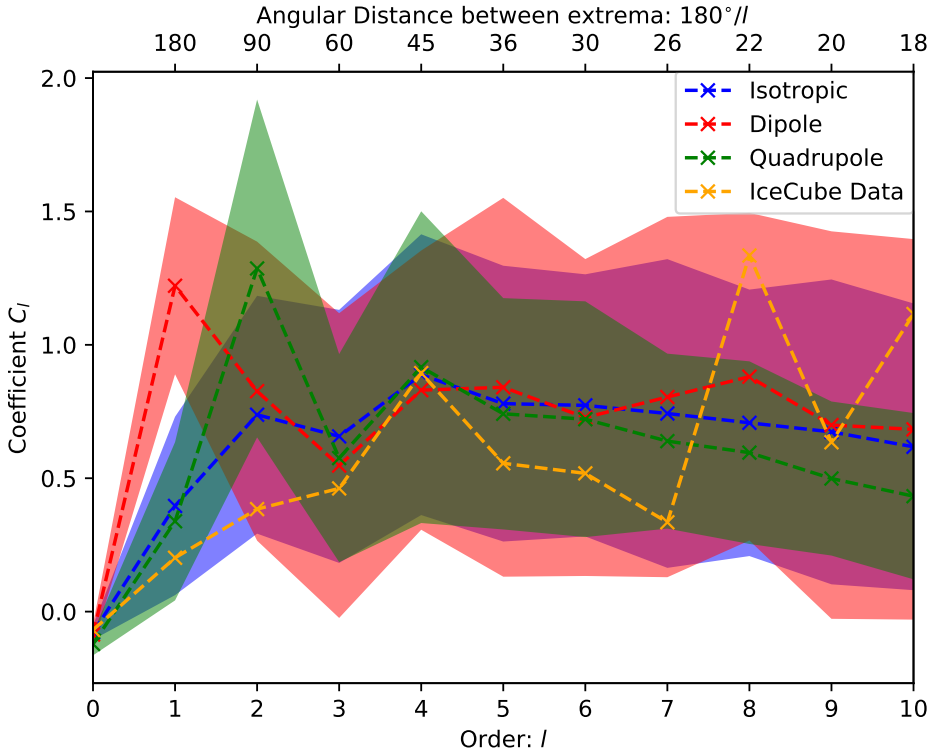

Figure 4.8: *Legendre coefficients from expansion of correlation function of pseudo-flux computed from IceCube data compared to statistical analysis of simulated isotropic, dipole and quadrupole samples (100 samples analysed each)*

4.2 Modelling of Neutrino Flux from Cosmic Ray Interactions

As described in section 2.2, it is not clear how large the contribution from CR interactions with local interstellar medium to the total neutrino flux actually is. Here, we estimate the neutrino and photon flux emerging in different media based on several assumptions we have to meet (cf. section 4.2.2).

4.2.1 Interactions in Scope

The interactions we are interested in are collisions of cosmic ray nuclei with matter at rest up to a maximum distance from our solar system to the closest AGNs. This happens the same way within all length scales described in section 2.3 with the medium density and the cosmic ray spectrum being the only parameters dependent on position. Equation 4.3 provides the relation of a given density distribution $n(\boldsymbol{r})$ and a cosmic ray flux $\phi_\mathrm{p}(E_\mathrm{p})$ - as a function of particle energy

E_p - towards a secondary particle flux ϕ_i where i either stands for photons or neutrinos. For easier numerical integration the integral is expressed in terms of the scale variable $x = {}^{E_\mathrm{i}}/_{E_\mathrm{p}}$, that has to be integrated from 0 to 1 in order to cover all E_p larger than E_i, and the location vector $\boldsymbol{r}$ in respect to earth, integrated over the volume V of the considered region. In this equation $\sigma_\mathrm{inel}({}^{E_\mathrm{i}}/x)$ defines the inelastic cross section of nucleon-nucleon interactions and the factor ${}^{1}/_{|\boldsymbol{r}|^2}$ takes in account how the flux of a source emitting homogeneously in all direction decreases with distance to the source. $F_\mathrm{i}(x, {}^{E_\mathrm{i}}/x)$ is the total and inclusive cross section that gives the probability density of the product i to occur at energy E_i with a nucleon energy ${}^{E_\mathrm{i}}/x$. Its exact form for both, gamma-rays and neutrinos, as well as the function for the cross section σ_inel used later on can be found in appendix B (Kelner, Aharonian and Bugayov 2006).

$$\phi_\mathrm{i}(E_\mathrm{i}) = \int_V \int_0^1 n(\boldsymbol{r})\sigma_\mathrm{inel}({}^{E_\mathrm{i}}/x)\phi_\mathrm{p}({}^{E_\mathrm{i}}/x)F_\mathrm{i}(x, {}^{E_\mathrm{i}}/x)\frac{1}{|\boldsymbol{r}|^2}\mathrm{d}x\mathrm{d}^3r \tag{4.3}$$

4.2.2 Simplifications Used

Everything should be made as simple as possible, but not simpler.

– Albert Einstein

In this thesis, the assumptions on the neutrino production in cosmic ray interactions are the following. Note that these simplifications can provide both, over- and underestimations of the resulting flux.

1. Interactions are reduced to proton-proton collisions with cosmic ray particles following the energy per nucleon spectrum. Proton interactions with CMB photons are neglected. Both may underestimate the neutrino flux as the CR spectrum is only considered partially and not all possible interactions are taken in account.

2. The cosmic-ray spectrum is assumed to be unique throughout the Milky Way. Local enhancements or attenuations are not considered. Furthermore, the spectrum of CR outside the solar system is barely known.

3. The total and inclusive cross sections F_i as well as the inelastic proton-proton cross section σ_inel are fits to data extracted from simulations done with the SIBYLL code (cf. Fletcher et al. 1994).

4. All volumes are approximated to spherical shells with constant density in the interior of the shell boundaries. This approximation assumed isotropy in the first place, and may produce more neutrino flux from several asymmetric distributions, e.g. the galactic plane.

5. Additionally the Earth is placed at the centre of each sphere. This as well assumes isotropy and may produce asymmetric distributions, e.g. the Local Bubble.

From assumptions 2, 4 and 5 a far less difficult integral than equation 4.3 follows, where the flux dependent and the spatial component splits into two integrals. This way the calculated flux is the same for any point, solely scaled by a factor given by size and density of the medium. After the straight forward evaluation of the spatial integral in spherical coordinates one finds

$$\phi_{\mathrm{i,m}}(E_\mathrm{i}) = 4\pi n_\mathrm{m}(R_\mathrm{m} - r_\mathrm{m}) \int_0^1 \sigma_\mathrm{inel}({}^{E_\mathrm{i}}/x)\phi_\mathrm{p}({}^{E_\mathrm{i}}/x)F_\mathrm{i}(x, {}^{E_\mathrm{i}}/x)\mathrm{d}x,$$

where $\phi_{\mathrm{i,m}}$ is the flux for medium m with density n_{m} and R_{m} and r_{m} are th shell boundaries.

Table 4.1 shows how each volume was included into calculations. Rather than treating the Local Cloudlets as separate objects, they are approximated as one big cloud. This is motivated by the fact that in relation to their size all of them are rather close-by (distance $< 15\,\mathrm{pc}$ at radii of 5 pc to 10 pc). Also the Milky Way interstellar medium is simplified by instead of separating the Disc and Halo into two objects the whole is treated as one with homogeneous density. The intergalactic medium we are interested in is up to distances where the closest AGNs are. Estimates are made using the information provided in section 2.3.

Table 4.1: *Geometric simplifications used for spatial integration*

Medium	Range	Density (cm^{-3})
Interplanetary Medium	50 km - 10^{10} km	10^{-2}
Local Cloudlets and Fluff	10^{10} km - 10 pc	10^{-1}
Local Bubble (interior)	10 pc - 150 pc	10^{-2}
Local Bubble (envelope)	150 pc - 155 pc	10^{3}
Milky Way (Interstellar Medium)	155 pc - 15 kpc	10^{-2}
Intergalactic Medium	15 kpc - 4 Mpc	10^{-6}

These assumptions are discussed further in chapter 5.

4.2.3 Fluxes for different Distances from Solar System

Figure 4.9 shows the result of this in comparison to the flux calculated from IceCube data using Poisson likelihood as shown in section 4.1.2. The total flux - that would be the sum of the six coloured lines - is not shown for the curve would cover the part coming from the Local Bubble envelope due to the total flux being highly dominated by it (see table 4.2). Also the flux from the interplanetary medium is not shown to its full extent in order to still being able to see the spectral shape of all other curves. However, the only difference to others only is the amplitude, the shape stays the same. As a measure, how well the IceCube data is described by the model, the reduced chi-squared is determined as 0.4 (cf. section A.1.4). Also the number of events predicted by the model can be calculated by integration of equation 4.1 with the modelled flux. This way one would expect 53.8 neutrinos between 10 TeV and 2 PeV within the duration of 1418 days. As it is interesting to know how much of the total flux is caused by each medium this is shown in table 4.2.

Table 4.2: *Percentage of total flux caused by each considered medium*

Medium	Share of total Flux(%)
Interplanetary Medium	<0.01
Local Cloudlets and Fluff	0.02
Local Bubble (interior)	0.03
Local Bubble (envelope)	97.00
Milky Way (Interstellar Medium)	2.88
Intergalactic Medium	0.08

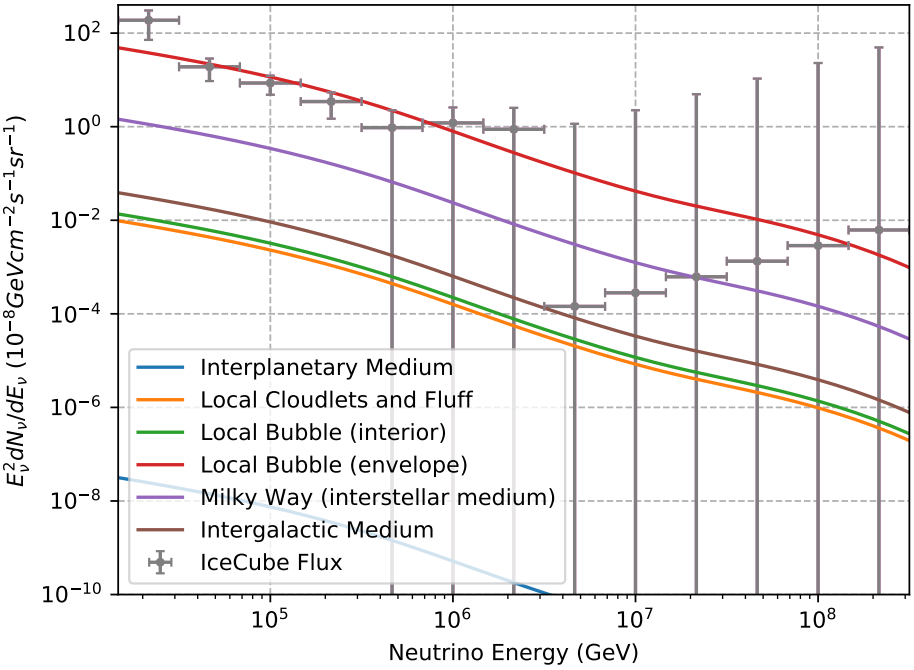

Figure 4.9: *Flux calculated from equation 4.3 for all media considered compared to flux from IceCube, cf. figure 4.7*

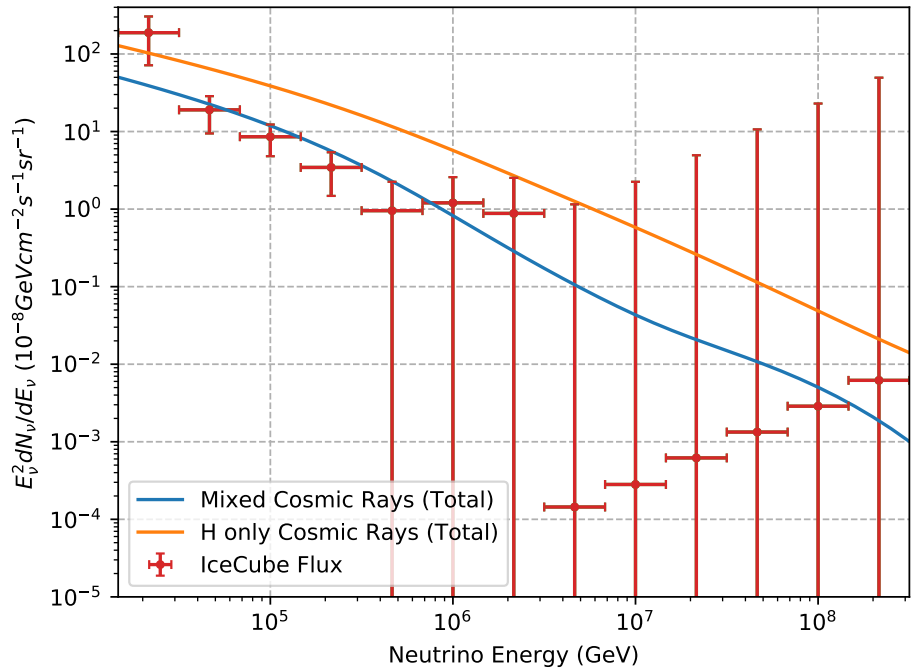

Figure 4.10: *Comparison between total neutrino flux from cosmic ray consisting of protons only (orange) or different nuclei (blue) interacting with surrounding matter and flux from IceCube, cf. figure 4.7*

4.2.4 Influences on Result caused by assumptions on Cosmic Ray Spectrum

As mentioned in chapter 3, currently it is only possible to detect the particle energy of cosmic rays in the energy realm we are interested in but not their charge number. Hence the influence of their composition on the outcome of our expected flux is of high interest and can be seen in figure 4.10 where the total flux of what we have calculated in section 4.2.3 is compared to the flux one gets with the same calculations, but instead of using a cosmic ray flux of different components, it is assumed to be solely made up of protons. Again the flux calculated from IceCube data is added in the plot for comparison.

4.2.5 Consistency Calculation: Oscillation Length

One aspect that needs to be treated is what characteristic lengths for neutrino oscillations are to be expected. If the size of the main source of neutrinos is much larger than the oscillation length it is most likely to detect similar numbers of each neutrino flavour. Otherwise the origin imprints the counts in such a way that out of three neutrinos two should be muon flavoured and one should be an electron neutrino. The ratio of neutrinos compared to that of antineutrinos should still be approximately one. However, with the IceCube setup this cannot be determined at the moment.

As explained in section 2.1.6 the oscillation length between two flavours, which suffices as a measure for order of magnitude, is given by

$$L_{\mathrm{osc}} = 4\pi \frac{\hbar p c^2}{\Delta m^2 c^4}.$$

The relevant length scale thus is given at highest occurring neutrino energies (so $pc \approx E = 100\,\mathrm{PeV}$) and the lowest Δm^2 which is given by $\Delta m^2_{12} c^4 = 7.37 \cdot 10^{-5}\,\mathrm{eV}^2$ (Tanabashi et al. 2018). With these parameters L_{osc} turns out to be around $3 \cdot 10^{15}\,\mathrm{m} \approx 0.1\,\mathrm{pc}$ which is less than a tenth of the distance between the Sun and the closest other star, Proxima Centauri (Unsöld and Baschek 2002). Hence, this would only show an effect, if the neutrinos would predominantly come from the solar system.

4.2.6 Diffuse Gamma-Ray Spectrum

With a slightly different $F(x, E_{\mathrm{p}})$ to that of neutrinos, that is also be shown in detail in appendix B, one can calculate the diffuse gamma spectrum emerging with neutrinos in cosmic ray interactions. For the calculation of the emerging flux the same assumptions as for neutrinos described in section 4.2.2 were applied.

In section 2.1.4.3 it was mentioned, that when travelling over cosmological distances these gammas via pair production on CMB photons can be converted down to a diffuse X-ray spectrum. However, due to the fact that as seen in table 4.2 the highest contribution to the flux is expected to come from distances of around 150 pc this effect was neglected. Figure 4.11 shows the result of these calculations, again separated into the different places of origin and again without the total flux, that would cover the flux from the Local Bubble envelope, and also scaled the same way as the neutrino spectrum in figure 4.9. Differences between the gamma and the neutrino spectrum are very hard to be seen with the naked eye which is why in figure 4.12 the ratio between the gamma and the neutrino flux is plotted over the interesting energy area from 10^5 GeV to 10^8 GeV.

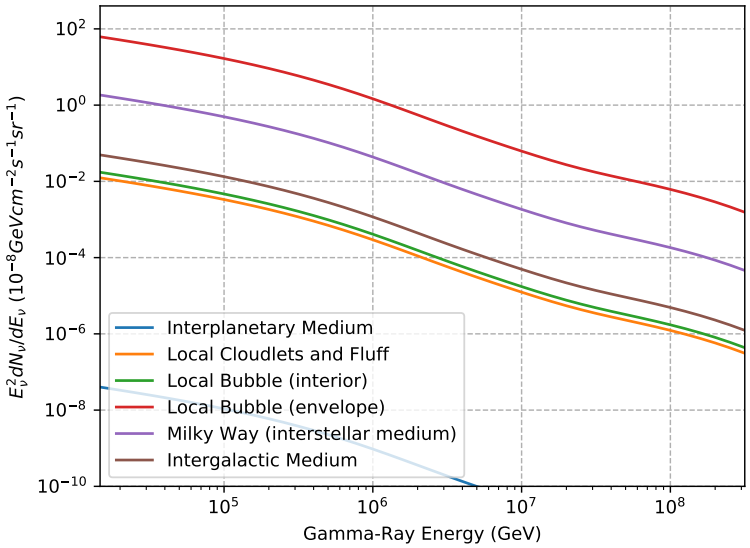

Figure 4.11: *Gamma-ray flux calculated from equation 4.3 for all media considered*

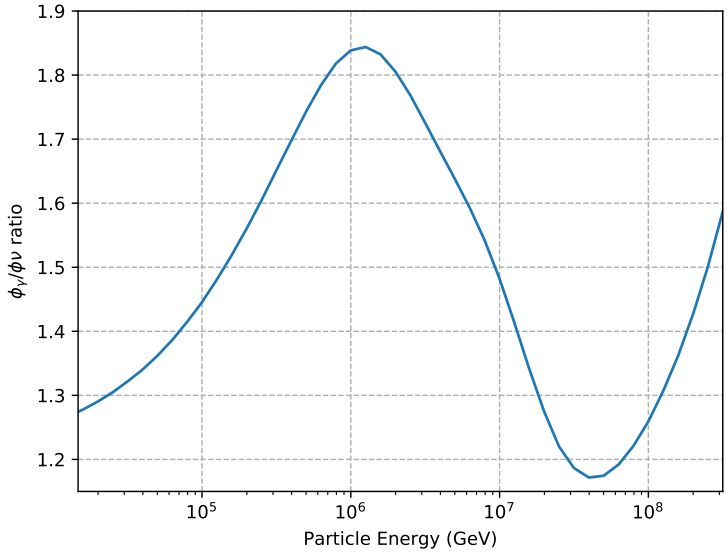

Figure 4.12: *Ratio between total gamma and neutrino fluxes calculated from cosmic ray interactions*

In comparison figure 4.13 shows the diffuse gamma-ray flux observed by the Fermi satellite up to 10 GeV and an extrapolation to higher energies published by Lipari and Vernetto 2018. Curve *a* shows the diffuse galactic gamma-ray flux observed by Fermi, where the dashed line is an extrapolation. Extragalactic gamma-rays observed by Fermi are represented by *b*. The regions *c*, *d*, and *e* then show estimates for the neutrino flux obtained by IceCube Collaboration et al. 2017 assuming an isotropic extragalactic flux .

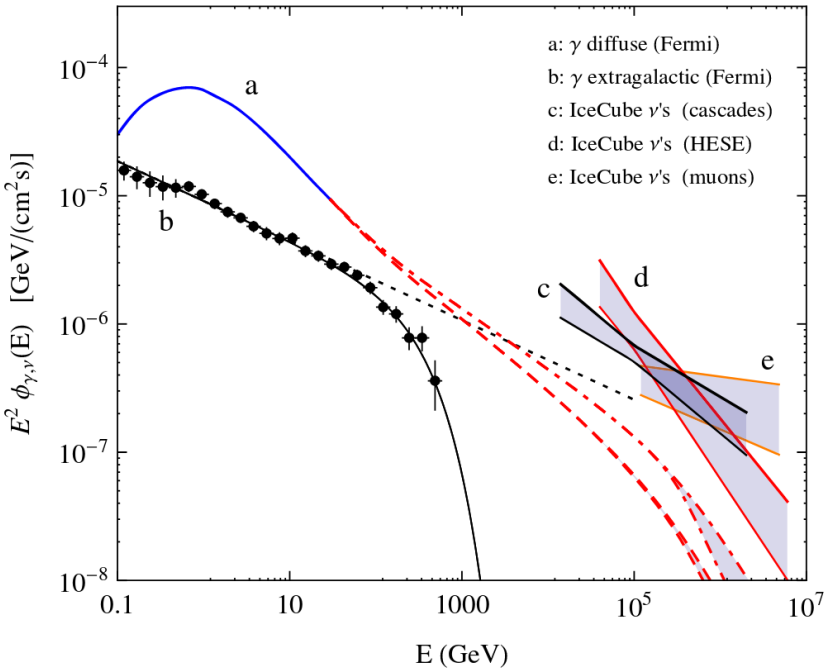

Figure 4.13: *Diffuse Gamma-Ray Spectrum observed by Fermi compared to neutrino flux estimated by IceCube (Lipari and Vernetto 2018)*

5

Discussion

This chapter will give an interpretation of the results, both of calculations done on IceCube data and on the theoretical fluxes from cosmic ray interactions.

As a start I want to give a quick summary on what in Aartsen et al. 2014 and similar papers was concluded from the data from IceCube. Next what calculations concerning this data done for this thesis can tell us and I will compare this new outcome to prior ones. The spectrum extracted this way will then help to analyse what can be expected from cosmic ray interactions as explained in section 4.2 where finally our assumptions made in the first place to obtain this flux will be tested concerning their plausibility.

5.1 Previous Interpretation

The first aspect that immediately attracts attention when looking at the data from IceCube is that the map of incidents does not at all look as maps like these seen in figure 2.6, which suggests that different to photons neutrinos do not mainly originate from sources spread all over the Milky Way and one needs to look for possible sources with an isotropic spatial distribution. Also for a very long time no statistically significant spatial correlation between any two or more events had been found which was interpreted as an indication of either many dim sources or one big source covering the whole sky. Due to many experiments like Super-Kamiokande detecting fluxes coming from the atmosphere one can probe this origin as a start. However, as stated in Aartsen et al. 2014 detecting down going atmospheric events (means neutrinos coming from the southern hemisphere) is disfavoured because generally neutrinos form together with muons. When falling in from above the detector they only have to pass the atmosphere and can trigger the anti-coincidence unit. Muons from the northern hemisphere on the other hand would have to penetrate Earth before reaching the detector which is much more unlikely. This means, that a flux predominantly originating in the atmosphere would not appear isotropic. Thus another possible source of neutrinos with energies that high was suggested to be blazars. These cosmological objects are believed to be origin of the highest energetic cosmic rays which, when interacting with matter, can form high energy neutrinos as explained in section 2.1.4.3. Due to very high energy gamma-rays being detected from various blazars the suggestion of these interactions appearing in the matter surrounding these accelerators naturally comes to mind. Additional fuel to this idea is given by an observation published 2018 in IceCube Collaboration et al. 2018a additionally, where several high energy neutrinos coming from one direction within a short period of time found to very likely be in correlation with a flare in gamma-rays detected from the blazar TXS 0506+056 which is the first multi-messenger event of very high energetic neutrinos and gamma-rays. Up until now this blazar presents the only neutrino source of significant spatial correlation.

Using data restricting atmospheric fluxes Aartsen et al. 2014 found the neutrino spectrum to follow a similar power law slope as that of cosmic rays predicted around supernova remnants. However, due to the low number of counts it is impossible to give a precise energy distribution which makes a proper comparison of these two spectra difficult (Aartsen et al. 2014).

5.2 Isotropy

Different to other studies done on IceCube data, in section 4.1.3 a direction independent measure of the flux isotropy was probed. Analysis as seen in 4.2 have the problem to carry the potential of being biased which means that they might overlook a possible anisotropy simply because they only test one direction. This new approach only checks whether there is a certain regularity in angles between each two events which makes it unbiased but of course takes away the chance of actually finding the actual spot of anisotropy, it only tests whether there is any.

From figure 4.8 we now learn, that as far as we can test it the neutrino flux actually seems to be isotropic. Pure dipoles and quadrupoles also for this low number of events already show their specific appearances clearly. However, when going to higher orders the isotropic flux, where all C_ls should be zero, also shows random patterns to occur regularly. Hence in order to do a better analysis by also including higher orders of anisotropy way more data points are needed. The Milky Way interstellar matter, which should contribute as something very similar to a quadrupole, can already be ruled out as a strong source. The Local Bubble however, which most likely has contributions at high multipole moment due to its complexity and large extension over the sky. Anyways, up until now this analysis is in accordance with what is suggested through other studies that the neutrino flux above 10 TeV is isotropic.

5.3 Spectrum

The sole difference between figures 4.7 and 4.6 using Poisson and Gaussian likelihood, due to it only being a first order estimate, are the error bars. Poisson likelihood should always be used for Poisson-distributed data, obeying counting statistics especially when dealing with a low number of counts, which is why they were then used as comparison later on. Results and uncertainties are similar to that in Aartsen et al. 2014. For low energies differences occur most likely due to not taking in account what one would expect from interactions in the Earth's atmosphere thus getting larger values. However, within the uncertainties those three analyses are consistent.

This most certainly also causes the steeper function one gets for the power law fit with a bigger negative power law index. For taking the atmosphere in account more data from IceTop would have been needed. Theoretically the model used to calculate the fluxes for different media around earth as done in 4.2 could have been used to characterize and contemplate influences by the atmosphere. However, the assumption of the laboratory being in the centre of the atmosphere is much farther off reality than with the other considered media. In addition the anti-coincidence unit IceCube uses causes a big anisotropy between the northern and the southern hemisphere which is hard to properly characterize. A second problem is that the atmospheric flux Aartsen et al. 2014 use for their analysis has a much steeper function than the data, which, if using our model, would not have occurred for as mentioned in section 4.2.3 all media share the same spectrum just differently scaled by their size and density.

With a proper prerequisite now we can analyse the results from section 4.2.

Do the Assumptions speak to us with a forked Tongue?

According to Gaisser 2012 reducing interactions of cosmic ray nuclei to proton-proton collisions is a good approximation to what one detects at high energies. Thus this first assumption should hold in any medium at any distance for what we want to find out. Including proton-gamma interactions however should increase the detailedness of the model and can be done following Kelner and Aharonian 2008.

Assumption two, that cosmic rays share the same spectrum in any medium given by that in the solar system, is more problematic, especially when going further away from the solar system.

Even at energies as high as relevant for us, cosmic rays can be bent by turbulent galactic magnetic fields and thus change significantly within the Milky Way. On top of that, the spectrum, at energies lower than where the Ankle is located, is believed to be caused by galactic sources like supernova remnants. Thus it might have been a better assumption to only use component three, which is supposedly the extragalactic component to cosmic ray flux, in the Intergalactic Medium which would reduce its contribution even more. How the flux from interaction within the Milky Way boundaries are effected by this is hard to guess, but at distances like the Local Bubble envelope and below no significant changes are supposed to appear at the relevant cosmic ray energies.

According to Kelner, Aharonian and Bugayov 2006 the inelastic cross section as well as the total and inclusive cross sections for both photons and neutrinos very well coincide with data from collision experiments and data taken from particle shower events in the atmosphere.

Assumptions 4 and 5, considering the geometry of the emission regions and the position of the Earth inside those, probably has the greatest influence on the flux. Especially the Milky Way and the solar system definitely do not have isotropic density distributions and we certainly are not in their centre. With a $1/R^2$ density distribution as function of the distance to the Sun neutrinos forming due to the Interplanetary Medium are supposed to mostly originate close to sun. For the Milky Way one would expect high anisotropies like those seen in 2.6. Each of the other media should at least as a first order approximation be well characterized by homogeneously dense spherical shells with the solar system in their centre.

Concluding, when receiving a significant amount of flux from either the medium except for the Local Bubble (interior or envelope) or the Local Cloudlets and Fluff would be problematic. Now given what we can see in figure 4.9 and table 4.2 indicates that our assumptions might be well chosen: The flux strongly is dominated by the envelope of the Local Bubble and follows a trend similar to that of the IceCube data. Even though the contribution from the Milky Way is the second largest it's already smaller by nearly two orders of magnitude which supposedly makes its effects of anisotropy insignificant at this low number of events. However, since the main interacting matter of the Milky way is located only in a very narrow range of latitude, a more detailed model considering this aspect as well is necessary for a better estimate of its relevance.

The IceCube flux is reproduced at a reduced chi-squared of 0.4, which in case of a fit would have indicated too many parameters. In this case it shows, that the observed spectrum is already well defined by a flux only from cosmic ray interactions in the local interstellar medium. As the number of events the model at the given assumptions predicts is 53.8 within the observation time and 52 were being observed, no contribution from distant sources like AGN would be necessary to explain the flux inferred by IceCube. However, this statement has to be seen as an upper limit for the contribution. Due to uncertainties in densities and boundaries a flux caused by distant sources is not ruled out,

What can additionally be taken into account to check the quality of assumptions is the correlated gamma-ray flux presented in section 4.2.6. At too high distances of above several 100 Mpc pair-production in CMB photons becomes relevant which will make the Intergalactic Medium opaque to gamma-rays at the energies we are interested in - 10 TeV to several PeV. Therefore we expect the diffuse gamma-ray flux at these energies to be caused by cosmic ray interactions with matter within the Milky. With proper assumption the total flux of gamma-rays we calculate should thus be of the same order of magnitude as the diffuse flux detected (Lipari and Vernetto 2018). Comparing 4.11 with measurements for example done by the Fermi satellite as shown in figure 4.13 this fits well. However, flux measurements done with Fermi only reach as far as 10 TeV, which is the lower boundary of what our models are designed for. Thus the flux we calculate can only be compared to extrapolations.

Two aspects not properly discussed yet are the cosmic ray composition concerning different nuclei and the influence of the uncertainty in thickness and density of the Local Bubble envelope. Figure 4.10 shows that in case of proton richer cosmic rays than assumed one gets a softer spectrum (with a lower absolute power law index) and thus also slightly higher flux values. However, taking into account cosmic ray compositions at lower energies and extrapolating these this case is disfavoured. The thickness and density on the other hand are parameters hard to detect. Both were taken from simulation data where the thickness varied by a factor of around two and the density by a factor of up to ten between different simulations. This indeed would significantly change the outcome with both being linear factor in the calculations. Still the flux from the Local Bubble envelope would be the most important contribution to the flux calculated from cosmic ray interactions and it would also still be a significant portion of what IceCube data suggests to be the total flux. As a minimum for what can be expected a good estimate is given by 5% of the total flux, which is given at a ten times smaller density and half the thickness in the Local Bubble envelope.

To put it in a nutshell, cosmic ray interactions with surrounding matter seem to play a significant role in creating the detected neutrino flux above 10 TeV and should definitely be included when one wants to estimate the flux we receive from more distant objects like blazars. According to the calculations with given assumptions the neutrino flux detected by IceCube could be explained by these cosmic ray interactions to its full extent.

5.4 Distance Measurement with Neutrinos

Additionally, I want to discuss whether or not it is possible to not only use neutrinos as messengers pointing towards cosmological events but also to determine the distance to them. The idea behind it is, that neutrino oscillations additionally to the distance to where they are created also depend on the energy. This would result in flavour-dependent energy-spectra, with the oscillations as functions of energy depend on the initial composition, and the distance to the source. Such an analysis would help in future neutrino experiments to identify sources.

The only cosmological objects emitting neutrinos at the highest energies detected by now are blazars. So let's assume the distance L be fixed with it being approximately 3.8 Mpc as the distance to Centaurus A. Now we can plot the flavour contribution over the energy range relevant to us using IceCube data, which can be seen in figure 5.1. One can't identify any oscillations as a function of energy due to the fact that the distance to this object is much farther away from us than the oscillation length for neutrinos of these energies would be. In figure 5.2 one can see how the energy dependent oscillations would look like in the more traceable distance of 10^{13} m in this energy realm when using the prior composition of $^2/_3$ muon neutrinos and $^1/_3$ electron neutrinos, as one would expect from proton-proton collisions as explained in section 2.1.4.3.

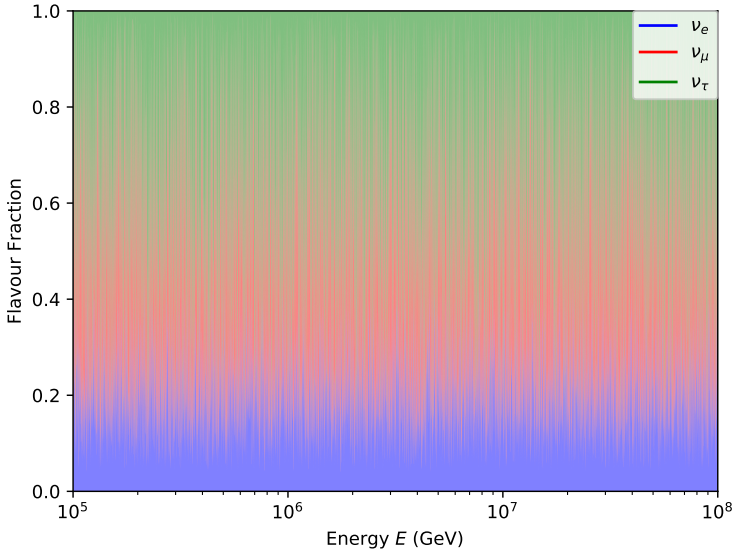

Figure 5.1: *Flavour fraction over energy, as received at Earth for a source at a distance of* 4,*Mpc with an initial composition of* 1/3 *electron and* 2/3 *muon neutrinos*

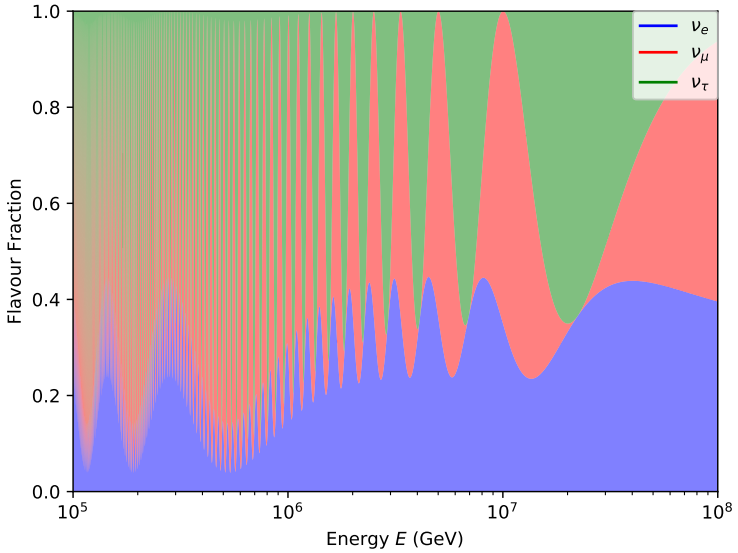

Figure 5.2: *Flavour fraction over energy, as received at Earth for a source at a distance of* 10^{13} *m with an initial composition of* 1/3 *electron and* 2/3 *muon neutrinos*

6

Summary, Conclusion and Prospect

6.1 Summary of Results and Conclusion

In this thesis, the IceCube data from 4 years of observation was analysed. First, an update on the IceCube results in Aartsen et al. 2014 with 30% more data is given. The flux approximately following a power law with spectral index of -3.4 being steeper than previous analyses of the IceCube collaboration still is consistent due to not taking an atmospheric component in account for this analysis. The previous finding of IceCube neutrinos being isotropically distributed has been questioned and investigated in an alternative way, by using an expansion in spherical harmonics. While higher order multipoles cannot be excluded due to the low number statistics, the IceCube data are consistent with isotropy, disfavouring dipole and quadrupole emission regions.

This isotropy was then investigated by modelling the neutrino flux as coming from cosmic ray interactions with ambient media. Based on assumptions on the interactions and the medium around Earth, estimates for fluxes of neutrinos and gamma-rays appearing at the same kind of interactions were calculated. It is shown that up to all of the IceCube neutrino flux can be accounted for in terms of local CR interactions at a calculated reduced chi-squared of 0.4, predominantly from the Local Bubble envelope, which as a neutrino source can be considered to be isotropic. This result must still be considered an upper limit, as simplifications and estimates for ambient media properties, such as density and shape, were used, which may decrease the contribution down to 5%. It is evident, however, that not only the absolute flux but also the shape of the neutrino spectrum is in perfect agreement with the IceCube measurements. In addition the diffuse gamma-ray spectrum, which is supposed to originate from such interactions within the Milky Way, also very well fits observations by the Fermi satellite.

Even though the multi-messenger event of the blazar TXS 0506+056 shows that neutrinos might be coincident with individual neutrino point sources, this study shows that a non-negligible fraction of the neutrino flux originates in the local environment and not in distant sources.

6.2 Prospect

Adding this model to previous calculations done will give more detailed constraints on extra-galactic neutrino fluxes, cosmic ray production rates and spectra at cosmological objects like blazars.

Including a more explicit description of the Local Bubble envelope will give better insight what neutrino flux we can expect from cosmic ray interactions. This means specifying the Bubble especially concerning thickness and density distribution across the sky as well as including smaller and bigger holes in the envelope - like for example the Chimney - in the calculations. The challenge in this task mostly lies in detecting and/or simulating in more detail for as soon as the density and thickness are known in order to receive the flux from a certain direction one only needs to integrate the product of thickness and density over the solid angle and multiply this by the spectral component. Using this correlation in reverse, IceCube can possibly also help determining a detailed shape of the Local Bubble.

On the other hand neutrinos from the Local Bubble envelope through this can also be used to study cosmic ray fluxes. A ten times bigger observatory then IceCube currently is being planned. With this a way more detailed and precise flux at higher energies hopefully paired with better angular resolution of events should be possible. With the correlation between the neutrino flux and the Local Bubble parameters one then could gain conclusion on the primary cosmic rays there.

Appendix A

Mathematical Methods

A.1 Maximum Likelihood Estimation

This section shall give a short introduction to statistical analysis as used during this thesis. The information given is taken from Press et al. 1992 and Cameron and Trivedi 1998.

A likelihood function is a function combining parameters of a statistical model with the data the model is supposed to describe. This can be used to find out, how well a model can describe the data. To determine best fitting parameters can be done by maximizing the likelihood. However, the likelihood function is dependent on what model one believes to describe the randomness of data best, whether it is for example distributed following a Gaussian or a Poisson law.

A.1.1 Probabilities

There are several different distributions random variables can follow. No matter the distribution one always wants some function to return the probability of a certain value to appear. Depending on whether the random variable is discrete or continuous one speaks of the probability mass or probability density function respectively. The probability mass function is used if a variable can only take on discrete values. At point x it returns the chance of the random variable to be x. In contrast to that the probability density function is used for continuously distributed random variables. It has to be integrated over an interval to return the probability of the random variable to be within this interval for the probability of it taking on one discrete value always is infinitesimally small.

A.1.2 Gaussian Distribution

The Gaussian (or normal) distribution is one of the most commonly used probability distribution. It is important especially due to the central limit theorem, which states that the mean values of variables drawn from any prior random distribution will converge towards a normal distribution at sufficiently high numbers of observations. Also many actual randomly distributed observations can approximately be described by a normal distribution. The Gaussian distribution is given by the expected value μ and the standard deviation σ as in equation A.1. Often a $1\,\sigma$ range is given for results which refers to a range within which the real result should lie in at around 68 % chance (the integral over equation A.1 from $-\sigma$ to σ). This however infers the random distribution to follow a Gaussian law which in general is not the case. In section A.1.5 the correct way of calculating uncertainties with a known distribution law is explained.

$$f(x)\mathrm{r}x = \frac{1}{\sqrt{2\pi\sigma^2}} \exp\left(-\frac{(x-\mu)^2}{2\sigma^2}\right) \mathrm{d}x \tag{A.1}$$

The Gaussian likelihood function P for a dataset with N data points is defined as in equation A.2 where y_i and x_i describe the data set, y describes the model which shall describe how y_i depend on the x_i. Additionally to x, y depends on parameters $a_1 ... a_\mathrm{M}$. The standard deviation or uncertainty of each y_i is given by σ_i. The term Δy describes a fixed range within which one

wants to determine the probability of y to be. This only is necessary if y_i can take on continuous values.

$$P \propto \prod_{i=1}^{N} \left\{ \exp\left[-\frac{1}{2} \left(\frac{y_\mathrm{i} - y(x_\mathrm{i})}{\sigma_\mathrm{i}} \right)^2 \right] \Delta y \right\} \tag{A.2}$$

A.1.3 Poisson Distribution

Poisson distributions have a strong relation with exponential distribution. If the probability of an event happening within $[t, t + \mathrm{d}t]$ is given by $\lambda \exp(-\lambda t)\mathrm{d}t$ (the exponential distribution probability density function), the number of events x happening until a time t follows a Poisson distribution with a probability mass function as in equation A.3. The expected value of such a distribution is given by λ. This distribution best describes experimental data that counts events.

$$\exp(-lambda)\frac{1}{x!}\lambda^\mathrm{x} \tag{A.3}$$

The Poisson likelihood function L for a dataset is given by equation A.4

$$L = \prod_{j=1}^{N} \frac{\exp[-y(x_\mathrm{i})][y(x_\mathrm{i})]^{y_\mathrm{i}}}{\Gamma(y_\mathrm{i} + 1)}, \tag{A.4}$$

where Γ is the gamma function.

A.1.4 Chi-Squared Fitting

With the logarithm being a strictly monotonous function instead of finding the maxima of the likelihoods given in sections A.1.2 and A.1.3 one can also maximize the natural logarithms of these functions. Furthermore since finding the maximum usually is harder than the minimum with a computer, the minimum of the negative logarithm can be determined in order to have the highest likelihood. Within these negative log-likelihoods there are several constant terms that don't have any effect on the result and are thus ignored. In case of the Gaussian distribution one receives the chi-squared function given by equation A.5. Doing the same for a Poisson distribution something like equation A.6 is the result one can use for fitting parameters to a curve.

$$\chi^2 = \sum_{i=1}^{N} \frac{(y_\mathrm{i} - y(x_\mathrm{i}))^2}{\sigma_\mathrm{i}^2} \tag{A.5}$$

$$-\ln L \propto \sum_{i=1}^{N} (y(x_\mathrm{i}) - y_\mathrm{i} \ln y(x_\mathrm{i})) \tag{A.6}$$

In order to find the best fitting parameters $a_1 ... a_\mathrm{M}$ one needs to find the minimum of the negative log-likelihood within the whole parameter space.

As a measure, how well a function fits data, one defines the reduced chi-squared

$$\chi^2_\mathrm{red} = \frac{\chi^2}{\nu},$$

where $\nu = N - M$ are the degrees of freedom. The reduced chi-squared should have a value of around 1. If it is too big, this means that the function does not yet fit the data well enough, if it is too small, this indicates that too many parameters were used and the fit becomes unnaturally good and thus unphysically. In section 4.2.3 this was done by using the first order calculation of the flux with Poissonian uncertainties as data. In order to include the non-symmetry of Poisson uncertainties the one according to the sign of deviation from each data point was used.

A.1.5 Parameter Uncertainties

As soon as we have our best fitting parameters, we want to find the uncertainties for our parameters at given data uncertainties. This again can be done using the negative log-likelihood. As shown in Press et al. 1992 each individual parameter uncertainty can be gained by determining the maximum value for the parameter within the multidimensional ellipsoid in the parameter space defined by the log-likelihood being less or equal to certain values. These values are given by δ solving the equation $\Gamma(\nu/2, \delta/2) = 1 - p$ where p is the probability one wants the value to be within the limits. In case of multiple parameters it is important to find the maximum of each parameter in the whole parameter space and not only along one axis!

A.2 Spherical Harmonics

The information given in this section can be found in Bennett et al. 2003.

When characterizing a periodic function one often develops it using sine and cosine functions decomposing the original one into different frequencies being multiples of the basic frequency, its harmonics. Something similar can be done with a function defined on a sphere, called spherical harmonics. Spherical harmonics play a major role on characterizing wave functions of electrons in atoms as well as characterizing spherically symmetries that can for example appear in electrodynamic systems. However, this also can be used the other way round to look for symmetries, for example in the flux we receive from the sky which was how they were used in this thesis.

Generally spherical harmonics are defined as

$$Y_{\mathrm{m}}^{\mathrm{l}}(\theta, \phi) = \sqrt{\frac{2l+1}{4\pi}\frac{(l-m)!}{(l+m)!}}\exp(im\phi)P_{\mathrm{l}}^{\mathrm{m}}(\cos\theta),$$

where l is a natural number (including 0) and $m \in -l, -l+1...l$ an integer and $P_{\mathrm{l}}^{\mathrm{m}}$ are the associated Legendre polynomials. These polynomials themselves are defined by the Legendre polynomials P_{l} by

$$P_{\mathrm{l}}^{\mathrm{m}}(x) = (-1)^{\mathrm{m}}(1-x^2)^{\mathrm{m}/2}\frac{\mathrm{d}^{\mathrm{m}}}{\mathrm{d}x^{\mathrm{m}}}(P_{\mathrm{l}}(x))$$

and

$$P_{\mathrm{l}}(x) = \frac{1}{2^{\mathrm{l}}l!}\frac{\mathrm{d}^{\mathrm{l}}}{\mathrm{d}x^{\mathrm{l}}}(x^2-1)^{\mathrm{l}}.$$

Any function $f(\theta, \phi)$ on a sphere can now be developed by spherical harmonics as

$$f(\theta, \phi) = \sum_{l=0}^{\infty}\sum_{m=-l}^{l} f_{\mathrm{l}}^{\mathrm{m}}Y_{\mathrm{m}}^{\mathrm{l}}(\theta, \phi)$$

where $f_{\mathrm{l}}^{\mathrm{m}}$ are coefficients.

One can for example use ${}^{\Delta\phi_{\mathrm{p}}(\theta,\phi)}/_{\phi_{\mathrm{p,\ mean}}}$ as $f(\theta, \phi)$. If we now do the expansion mentioned in equation 4.2

$$f(\cos\theta) = \left\langle \frac{\Delta\phi_{\mathrm{p}}(\boldsymbol{m})}{\phi_{\mathrm{p,\ mean}}}\frac{\Delta\phi_{\mathrm{p}}(\boldsymbol{n})}{\phi_{\mathrm{p,\ mean}}}\right\rangle = \sum_{l}\frac{2l+1}{4\pi}C_{\mathrm{l}}P_{\mathrm{l}}(\cos\theta)$$

what we receive as C_{l} are the variances of the $f_{\mathrm{l}}^{\mathrm{m}}$ over m as

$$\left\langle |f_{\mathrm{l}}|^2\right\rangle = \frac{1}{2l+1}\sum_{m=-l}^{l}|f_{\mathrm{l,m}}|^2 = C_{\mathrm{l}}.$$

Each C_{l} refers to the fraction of the pseudo-flux deviation that has its minima and maxima separated at mean distances of ${}^{180^\circ}/_{l}$.

Appendix B

Calculating Neutrino and Gamma Fluxes from Cosmic Ray Spectrum

This chapter will provide information on the model used for cosmic rays provided by Gaisser 2012 and the cross sections for inelastic proton-proton interactions resulting in gamma-ray photons and neutrinos, which Kelner, Aharonian and Bugayov 2006 derives.

B.1 Cosmic Ray Model

Above a total energy of around 100 TeV it is not possible to measure primary nuclei any more (cf. section 3). However, higher energy particles need to be considered when calculating a neutrino flux up to 2 PeV. Furthermore it is a good approximation to treat the interactions as collisions between individual nucleons in which the two involved nuclei having the energy of the total nucleus energies divided by the mass number A. This leads to the need of fitting the all-particle spectra detected with extrapolations for the five groups (Gaisser 2012).

Gaisser 2012 uses equation B.1 as general form for the flux caused by each group (i) containing all three components (j)

$$E\phi_{\mathrm{i}}(E) = \sum_{j=1}^{3} a_{\mathrm{i,j}} E^{-\gamma_{\mathrm{i,j}}} \exp\left[-\frac{E}{Z_{\mathrm{i}} R_{\mathrm{c,j}}}\right]. \tag{B.1}$$

$E\phi_{\mathrm{i}}$ defines $E \cdot {}^{\mathrm{d}N}/_{\mathrm{d}E}$ in units $\mathrm{m}^{-2}\mathrm{sr}^{-1}\mathrm{s}^{-1}$ with $a_{\mathrm{i,j}}$ in table B.1 of unit $\mathrm{GeV}^{\gamma_{\mathrm{i,j}}}\mathrm{m}^{-2}\mathrm{sr}^{-1}\mathrm{s}^{-1}$. R is the magnetic rigidity,

$$R = \frac{pc}{Ze},$$

with Ze the charge of the nucleus and the momentum p. That the rigidity defines the three components is due to propagation models in magnetised plasma only depend on this measure. Restricted for example by the accelerators size or expected magnetic fields, $Z_{\mathrm{i}} \cdot \mathrm{e} \cdot R_{\mathrm{C,j}}$ defines the cut-off energy of a spectral component j and group i which leads to the conclusion that cut-offs appear at lower energies for nuclei with lower charge numbers.

The parameters gained by Gaisser 2012 to experiment data can be seen in table B.1.

Table B.1: Cut-off rigidities $R_{\mathrm{C,j}}$, integral spectral indices $\gamma_{\mathrm{i,j}}$ and normalization constants $a_{\mathrm{i,j}}$ for equation B.1 (Gaisser 2012)

$\mathrm{e}R_{\mathrm{C}}$	γ	$a_{\mathrm{i,j}}$ p	He	CNO	Mg-Si	Mn-Fe
γ for Pop. 1	-	1.66	1.58	1.63	1.67	1.63
Population 1: 4 PeV	see line 1	7860	3550	2200	1430	2120
Population 2: 30 PeV	1.4	20	20	13.4	13.4	13.4
Population 3: 2 EeV	1.4	1.7	1.7	1.14	1.14	1.14

For a better understanding of how to properly use the parameters given in table B.1 the following gives the $E\phi$ used for CNO:

$$E\phi_{\mathrm{CNO}}\left(E\right) = 2200\frac{\mathrm{GeV}^{1.63}}{\mathrm{m}^2\cdot\mathrm{sr}\cdot\mathrm{s}}E^{-1.63}\exp\left[-\frac{E}{7\cdot 4\mathrm{PeV}}\right] +$$

$$13.4\frac{\mathrm{GeV}^{1.4}}{\mathrm{m}^2\cdot\mathrm{sr}\cdot\mathrm{s}}E^{-1.4}\exp\left[-\frac{E}{7\cdot 30\mathrm{PeV}}\right] + 1.14\frac{\mathrm{GeV}^{1.4}}{\mathrm{m}^2\cdot\mathrm{sr}\cdot\mathrm{s}}E^{-1.4}\exp\left[-\frac{E}{7\cdot 2\mathrm{EeV}}\right]$$

As seen in figure 2.2.3 the high energy part of the all particle spectrum is dominated by heavy nuclei. However, further calculations in this thesis need the energy per nucleon or rather the spectrum of protons instead, which both can be seen in figure B.1 (bottom left and top respectively). Those two spectra are obtained by replacing E on the right side of formula B.1 by $A\cdot E$ for the nucleon spectrum with the atomic number A and additionally multiplying these same spectra with Z/A in order to receive the proton spectrum. The bottom right graph, that gives the ratio of the groups of the total proton spectrum, shows that the entire spectrum is dominated by hydrogen. Plotting the same ratio for nucleons instead of protons looks similar. In equations B.2 and equation B.3 the spectra used for nuclei and protons can be seen respectively.

$$E\phi_{\mathrm{i}}\left(E\right) = A_{\mathrm{i}}\sum_{j=1}^{3} a_{\mathrm{i,j}}(A_{\mathrm{i}}E)^{-\gamma_{\mathrm{i,j}}}\exp\left[-\frac{A_{\mathrm{i}}E}{Z_{\mathrm{i}}R_{\mathrm{c,j}}}\right] \tag{B.2}$$

$$E\phi_{\mathrm{i}}\left(E\right) = Z_{\mathrm{i}}\sum_{j=1}^{3} a_{\mathrm{i,j}}(A_{\mathrm{i}}E)^{-\gamma_{\mathrm{i,j}}}\exp\left[-\frac{A_{\mathrm{i}}E}{Z_{\mathrm{i}}R_{\mathrm{c,j}}}\right] \tag{B.3}$$

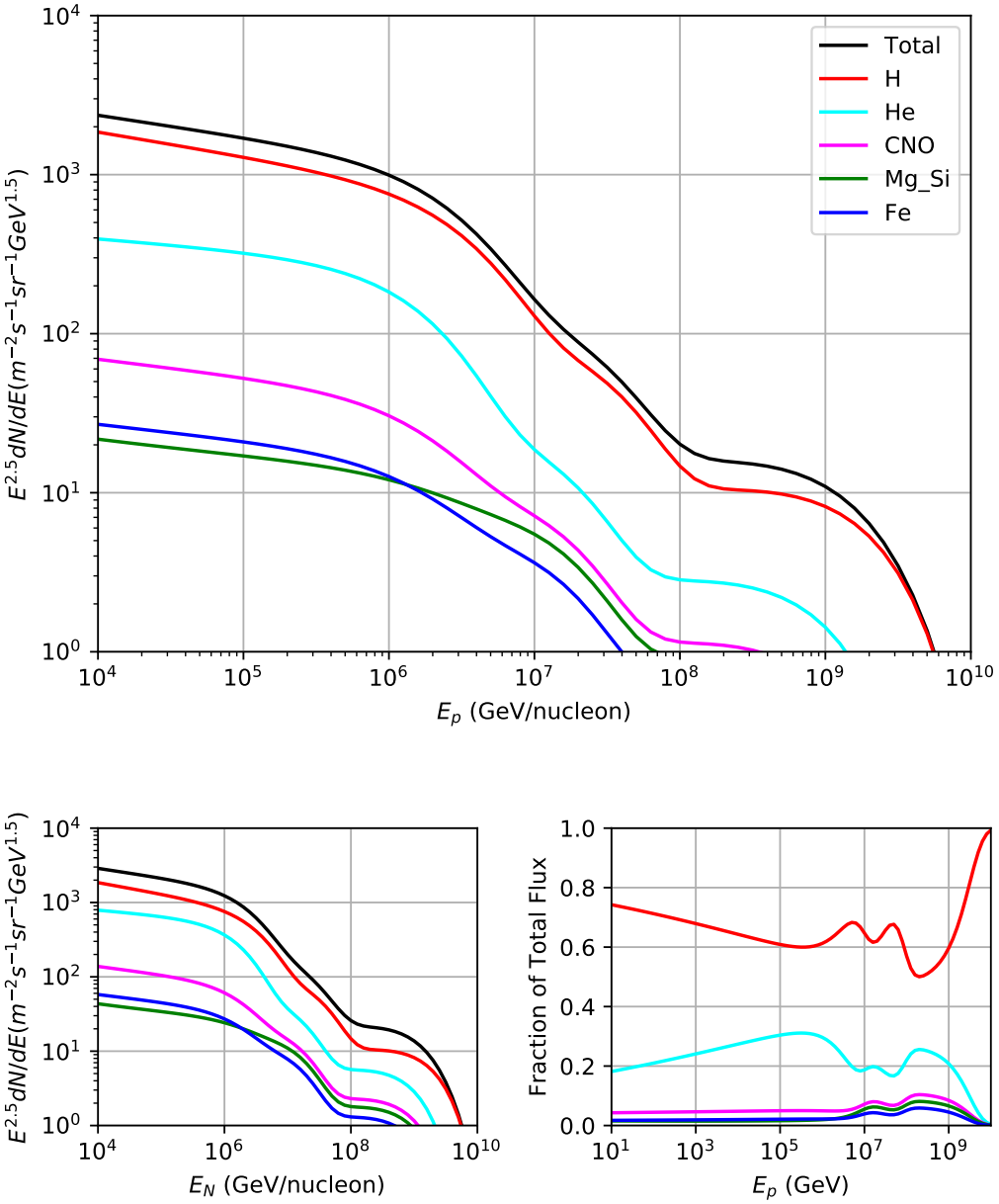

Figure B.1: *Top: energy per proton spectrum for all five groups obtained by taking atomic number and charge number in account*
Bottom left: energy per nucleon spectrum for all five groups obtained by taking atomic number in account
Bottom right: energy per nucleon fraction of total flux for all five groups

B.2 Cross Sections

With a given proton spectrum one needs the inelastic proton-proton cross section σ_{inel} as a function of proton energy E_{p}

$$\sigma_{\text{inel}}(E_{\text{p}}) = (34.2 + 1.88L + 0.25L^2) \cdot \left[1 - \left(\frac{E_{\text{th}}}{E_{\text{p}}}\right)^4\right]^2 \cdot \text{mb},$$

where $E_{\mathrm{th}} = (m_{\mathrm{p}} + 2m_{\pi} + {}^{m_{\pi}^2}/_{m_{\mathrm{p}}})\, c^2$ is the threshold energy for pion production, m_{p} the proton mass, m_{π} the pion mass and $L = \ln {}^{E_{\mathrm{p}}}/_{1\mathrm{TeV}}$. Figure B.2 visualizes this cross section.

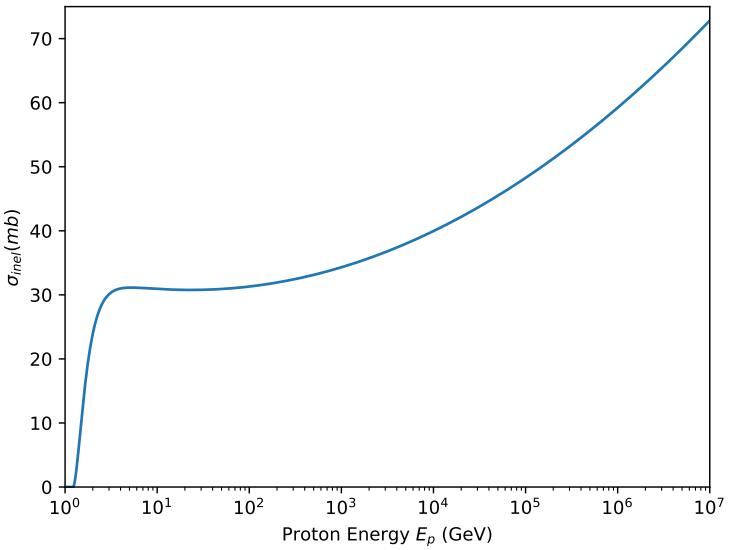

Figure B.2: *Inelastic cross section of proton-proton collisions in mb over proton energy*

Decay into Photons

How inelastically scattering protons then contribute to fluxes of photons and neutrinos is defined by the specific F_{i}. For photons this is given by

$$F_{\gamma}(x, E_{\mathrm{p}}) = B_{\gamma} \frac{\ln(x)}{x} \left(\frac{1 - x^{\beta_{\gamma}}}{1 + k_{\gamma} x^{\beta_{\gamma}} (1 - x^{\beta_{\gamma}})} \right)^4 \times$$

$$\left[\frac{1}{\ln(x)} - \frac{4\beta_{\gamma} x^{\beta_{\gamma}}}{1 - x^{\beta_{\gamma}}} - \frac{4 k_{\gamma} \beta_{\gamma} x^{\beta_{\gamma}} (1 - 2x^{\beta_{\gamma}})}{1 + k_{\gamma} x^{\beta_{\gamma}} (1 - x^{\beta_{\gamma}})} \right],$$

where the parameters B_{γ}, β_{γ} and k_{γ} are given as

$$B_{\gamma} = 1.30 + 0.14L + 0.011L^2,$$

$$\beta_{\gamma} = \frac{1}{1.79 + 0.11L + 0.008L^2},$$

$$k_{\gamma} = \frac{1}{0.801 + 0.049L + 0.014L^2}.$$

Decay into Neutrinos

As explained in section 2.1.4 charged pions usually first decay into muons via a two particle decay. This decay can be characterized similarly to that into photons as

$$F_{\nu_{\mu}1}(x, E_{\mathrm{p}}) = B' \frac{\ln(x)}{x} \left(\frac{1 - x^{\beta'}}{1 + k' x^{\beta'} (1 - x^{\beta'})} \right)^4 \times$$

$$\left[\frac{1}{\ln(x)} - \frac{4\beta' x^{\beta'}}{1 - x^{\beta'}} - \frac{4 k' \beta' x^{\beta_{\gamma}} (1 - 2x^{\beta'})}{1 + k' x^{\beta'} (1 - x^{\beta'})} \right],$$

with a sharp cut-off at $x \geq 0.427$ due to decay dynamics. The parameters B', β' and k' are given as

$$B' = 1.75 + 0.204L + 0.010L^2,$$
$$\beta' = \frac{1}{1.67 + 0.111L + 0.0038L^2},$$
$$k' = 1.07 - 0.086L + 0.002L^2.$$

The muon then decays further into an electron/positron, one electron like neutrino and a muon like neutrino. Each of these three particles follows a similar law which is given as

$$F_{\mathrm{e}}(x, E_{\mathrm{p}}) = B_{\mathrm{e}} \frac{(1 + k_{\mathrm{e}}(\ln x)^2)^3}{x\,(1 + {}^{0.3}/_{x^{\beta_{\mathrm{e}}}})} (-\ln(x))^5,$$

where

$$B_{\mathrm{e}} = \frac{1}{69.5 + 2.65L + 0.3L^2}$$
$$\beta_{\mathrm{e}} = \frac{1}{(0.201 + 0.062L + 0.00042L^2)^{1/4}},$$
$$k_{\mathrm{e}} = \frac{0.279 + 0.141L + 0.0172L^2}{0.3 + (2.3 + L)^2}.$$

Altogether F_ν thus is given by $F_\nu = F_{\nu_\mu 1} + 2 \cdot F_{\mathrm{e}}$. Figure B.3 shows the three $x^2 F_{\mathrm{i}}$ for photons and the different neutrino flavours as well as the sum for all neutrinos emerging from pion decays at a given proton energy of $E_{\mathrm{p}} = 0.1\,\mathrm{TeV}$.

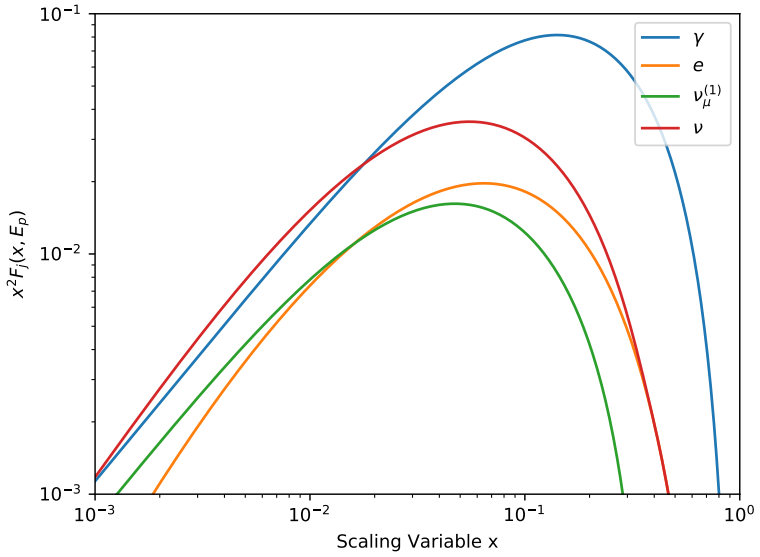

Figure B.3: *Energy dependent F_{i} for neutrinos and gammas from pion decays at proton-proton collisions with a cosmic ray energy of $E_{\mathrm{p}} = 0.1$ TeV*

Including the creation of η mesons from proton-proton increases all calculated fluxes by less than 10 % with a lower deviation at higher x and thus neutrino/photon energies, which is why this effect was ignored with other assumptions supposedly having bigger impacts.

Appendix C

Mapping the Sky

This chapter was written using information given in Poleski 2013 and Unsöld and Baschek 2002.

When looking up in the night sky one only gets a slight idea of how many objects there are out in the universe. In order to do proper observations, catalogues of these objects are necessary. Especially their location plays a major role. This can be done using different reference frames called celestial coordinate systems. For this thesis two of them were of special interest, equatorial and galactic coordinates.

Equatorial coordinates only use parameters defined by Earth and its orbit around the Sun to describe the position of objects on the celestial sphere (a sphere to project all celestial objects on). The celestial equator of this coordinate system is defined by the projection of the Earth's equator. Same goes for north and south pole. A star's position perpendicular to the equator is called declination δ (abbreviation dec) and is measured in positive degrees towards the north pole and in negative degrees when it is located on the southern hemisphere. As equivalent of terrestrial longitude one uses the right ascension α (abbreviation RA) and its zero point on the equator is defined by the location of the Sun when it crosses the March equinox[1]. Right ascension is measured in hours, minutes and seconds. This concept of cartography often is used for earthbound detectors due to its simple calibration. However, due to effects like nutation and precession of the Earth's axis this coordinate system is time dependent which makes it important to give the reference date of an object's location.

In galactic coordinates the celestial equator is the projection of the galactic plane onto the celestial sphere, and the primary direction points towards the direction of the Milky Way centre. Currently Sculptor, a small star constellation, represents the galactic south pole, Coma Berenices the north pole. This definition has changed a couple of times already though, which makes the time of observation important as well. The galactic coordinate system especially is of interest when one clearly wants to see what can be accounted to effects caused by the Milky Way.

Since the time dependent conversion between these two coordinate systems is not trivial for this thesis a python packages from "astropy" called "SkyCoord" was used for transformation.

[1] This is defined by the instant when the Sun passes through an imaginary extension of Earth's equator.

References

Aartsen, M. G. et al. (2014). »Observation of High-Energy Astrophysical Neutrinos in Three Years of IceCube Data«. In: *Physical Review Letters* 113.10, 101101, p. 101101. DOI: 10.1103/PhysRevLett.113.101101. arXiv: 1405.5303 [astro-ph.HE].

Aartsen, M. G. et al. (2017a). »Constraints on Galactic Neutrino Emission with Seven Years of IceCube Data«. In: ApJ 849, 67, p. 67. DOI: 10.3847/1538-4357/aa8dfb. arXiv: 1707.03416 [astro-ph.HE].

Aartsen, M. G. et al. (2017b). »The Contribution of Fermi-2LAC Blazars to Diffuse TeV-PeV Neutrino Flux«. In: ApJ 835, 45, p. 45. DOI: 10.3847/1538-4357/835/1/45. arXiv: 1611.03874 [astro-ph.HE].

Aartsen, M. G. et al. (2017c). »The IceCube Neutrino Observatory: instrumentation and online systems«. In: *Journal of Instrumentation* 12, P03012. DOI: 10.1088/1748-0221/12/03/P03012. arXiv: 1612.05093 [astro-ph.IM].

Abbott, B. P. et al. (2017). »Multi-messenger Observations of a Binary Neutron Star Merger«. In: ApJ 848, L12, p. L12. DOI: 10.3847/2041-8213/aa91c9. arXiv: 1710.05833 [astro-ph.HE].

Ahlers, M. and F. Halzen (2014). »Pinpointing extragalactic neutrino sources in light of recent IceCube observations«. In: Phys. Rev. D 90.4, 043005, p. 043005. DOI: 10.1103/PhysRevD.90.043005. arXiv: 1406.2160 [astro-ph.HE].

Alfaro, E. J., E. Pérez and J. Franco, eds. (2004). *How Does the Galaxy Work?* Vol. 315. Astrophysics and Space Science Library. DOI: 10.1007/1-4020-2620-X.

Andersen, K. J., M. Kachelriess and D. V. Semikoz (2018). »High-energy Neutrinos from Galactic Superbubbles«. In: ApJ 861, L19, p. L19. DOI: 10.3847/2041-8213/aacefd. arXiv: 1712.03153 [astro-ph.HE].

Andres, E. et al. (2000). »The AMANDA neutrino telescope: principle of operation and first results«. In: *Astroparticle Physics* 13, pp. 1–20. DOI: 10.1016/S0927-6505(99)00092-4. eprint: astro-ph/9906203.

Andrews, D. G. (2010). *An Introduction to Atmospheric Physics*. 2nd ed. Cambridge University Press. DOI: 10.1017/CBO9780511800788.

Anicin, I. V. (2005). »The Neutrino - Its Past, Present and Future«. In: *ArXiv Physics e-prints*. eprint: physics/0503172.

Arnett, W. D. et al. (1989). »Supernova 1987A«. In: ARA&A 27, pp. 629–700. DOI: 10.1146/annurev.aa.27.090189.003213.

Atwood, W. B. et al. (2009). »The Large Area Telescope on the Fermi Gamma-Ray Space Telescope Mission«. In: ApJ 697, pp. 1071–1102. DOI: 10.1088/0004-637X/697/2/1071. arXiv: 0902.1089 [astro-ph.IM].

Bellerive, A. (2004). »Review of Solar Neutrino Experiments«. In: *International Journal of Modern Physics A* 19, pp. 1167–1179. DOI: 10.1142/S0217751X04019093. eprint: hep-ex/0312045.

Bennett, C. L. et al. (2003). »First-Year Wilkinson Microwave Anisotropy Probe (WMAP) Observations: Preliminary Maps and Basic Results«. In: ApJS 148, pp. 1–27. DOI: 10.1086/377253. eprint: astro-ph/0302207.

Bergström, L. and A. Goobar (2006). *Cosmology and Particle Astrophysics*. 2nd ed. Springer-Verlag. ISBN: 3-540-32924-2.

Billard, J., E. Figueroa-Feliciano and L. Strigari (2014). »Implication of neutrino backgrounds on the reach of next generation dark matter direct detection experiments«. In: Phys. Rev. D 89.2, 023524, p. 023524. DOI: 10.1103/PhysRevD.89.023524. arXiv: 1307.5458 [hep-ph].

Britto, R. J. et al. (2016). »Multiwavelength Study of Fermi-LAT blazars Variability and Radiation Production Mechanisms«. In: *SF2A-2016: Proceedings of the Annual meeting of the French Society of Astronomy and Astrophysics*. Ed. by C. Reylé et al., pp. 93–101.

Brown, L. M. (2008). »The Idea of the Neutrino«. In: *Physics Today* 31, pp. 23–28. URL: https://physicstoday.scitation.org/doi/10.1063/1.2995181.

Cameron, A. C. and P. K. Trivedi (1998). *Regression Analysis of Count Data*. 1st ed. Cambridge University Press. ISBN: 0 521 63201 3.

Clemens, D. P. (1985). »Massachusetts-Stony Brook Galactic plane CO survey - The Galactic disk rotation curve«. In: ApJ 295, pp. 422–428. DOI: 10.1086/163386.

Cowan, Jr. C. L. et al. (1956). »Detection of the Free Neutrino: A Confirmation«. In: *Science* 124, pp. 103–104. DOI: 10.1126/science.124.3212.103.

Davis, Jr. R. and J. N. Bahcall (1969). »Review Paper: Solar Neutrinos.« In: *Bulletin of the American Astronomical Society*. Vol. 1. BAAS, p. 339.

Davis, Jr. R., A. K. Mann and L. Wolfenstein (1989). »Solar neutrinos.« In: *Annual Review of Nuclear and Particle Science* 39, pp. 467–506. DOI: 10.1146/annurev.ns.39.120189.002343.

Davis, R., D. S. Harmer and K. C. Hoffman (1968). »Search for Neutrinos from the Sun«. In: *Physical Review Letters* 20, pp. 1205–1209. DOI: 10.1103/PhysRevLett.20.1205.

Dazzi, F. et al. (2015). »Performance studies of the new stereoscopic Sum-Trigger-II of MAGIC after one year of operation«. In: *ArXiv e-prints*. arXiv: 1508.05255 [astro-ph.IM].

de Angelis, A. et al. (2009). »Photon propagation and the very high energy γ-ray spectra of blazars: how transparent is the Universe?« In: MNRAS 394, pp. L21–L25. DOI: 10.1111/j.1745-3933.2008.00602.x. arXiv: 0807.4246.

Diehl, R. (2013). »Nuclear astrophysics lessons from INTEGRAL«. In: *Reports on Progress in Physics* 76.2, 026301, p. 026301. DOI: 10.1088/0034-4885/76/2/026301. arXiv: 1302.3441 [astro-ph.HE].

Fletcher, R. S. et al. (1994). »sibyll: An event generator for simulation of high energy cosmic ray cascades«. In: Phys. Rev. D 50, pp. 5710–5731. DOI: 10.1103/PhysRevD.50.5710.

Follin, B. et al. (2015). »First Detection of the Acoustic Oscillation Phase Shift Expected from the Cosmic Neutrino Background«. In: *Phys. Rev. Lett.* 115 (9), p. 091301. DOI: 10.1103/PhysRevLett.115.091301. URL: https://link.aps.org/doi/10.1103/PhysRevLett.115.091301.

Gaia Collaboration et al. (2018). »Gaia Data Release 2. Summary of the contents and survey properties«. In: A&A 616, A1, A1. DOI: 10.1051/0004-6361/201833051. arXiv: 1804.09365.

Gaisser, T. K. (2012). »Spectrum of cosmic-ray nucleons, kaon production, and the atmospheric muon charge ratio«. In: *Astroparticle Physics* 35, pp. 801–806. DOI: 10.1016/j.astropartphys.2012.02.010. arXiv: 1111.6675 [astro-ph.HE].

Granados, A. et al. (2017). »GalRotpy: an educational tool to understand and parametrize the rotation curve and gravitational potential of disk-like galaxies«. In: *ArXiv e-prints*. arXiv: 1705.01665.

Grotz, K. and H. V. Klapdor (1989). *Schwache Wechselwirkung in Kern-, Teilchen- und Astrophysik*. Stuttgart: Vieweg+Teubner Verlag. ISBN: 3-529-03035-7.

Halzen, F. and A. D. Martin (1984). *Quarks and Leptons*. New York: Wiley. Chap. 1. ISBN: 0471887412, 9780471887416.

Harris, G. L. H. (2010). »NGC 5128: The Giant Beneath«. In: PASA 27, pp. 475–481. DOI: 10.1071/AS09063. arXiv: 1004.4907.

HI4PI Collaboration et al. (2016). »HI4PI: A full-sky H I survey based on EBHIS and GASS«. In: A&A 594, A116, A116. DOI: 10.1051/0004-6361/201629178. arXiv: 1610.06175.

Hillas, A. M. (2006). »Cosmic Rays: Recent Progress and some Current Questions«. In: *ArXiv Astrophysics e-prints*. eprint: astro-ph/0607109.

IceCube Collaboration (2013). »Evidence for High-Energy Extraterrestrial Neutrinos at the IceCube Detector«. In: *Science* 342, 1242856, p. 1242856. DOI: 10.1126/science.1242856. arXiv: 1311.5238 [astro-ph.HE].

– (2015). *Observation of Astrophysical Neutrinos in Four Years of IceCube Data (released 21 Oct 2015)*. https://icecube.wisc.edu/science/data/HE-nu-2010-2014. Accessed: 14-08-2018.

IceCube Collaboration et al. (2017). »The IceCube Neutrino Observatory - Contributions to ICRC 2017 Part II: Properties of the Atmospheric and Astrophysical Neutrino Flux«. In: *arXiv e-prints*, arXiv:1710.01191, arXiv:1710.01191. arXiv: 1710.01191 [astro-ph.HE].

IceCube Collaboration et al. (2018a). »Multimessenger observations of a flaring blazar coincident with high-energy neutrino IceCube-170922A«. In: *Science* 361, eaat1378, eaat1378. DOI: 10.1126/science.aat1378. arXiv: 1807.08816 [astro-ph.HE].

IceCube Collaboration et al. (2018b). »Neutrino emission from the direction of the blazar TXS 0506+056 prior to the IceCube-170922A alert«. In: *Science* 361, pp. 147–151. DOI: 10.1126/science.aat2890. arXiv: 1807.08794 [astro-ph.HE].

JACEE Collaboration (1997). »Cosmic Ray Proton and Helium Spectra - Results from JACEE«. In: *International Cosmic Ray Conference* 4, p. 1.

Joutsenvaara, J. (2016). *Deeper Understanding at Lab 2:...* https://www.researchgate.net/publication/304487324_DEEPER_UNDERSTANDING_AT_LAB_2_THE_NEW_EXPERIMENTAL_HALL_AT_CALLIO_LAB_UNDERGROUND_CENTRE_FOR_SCIENCE_AND_R_D_IN_THE_PYHASALMI_MINE_FINLAND. [Online; accessed 29-October-2018].

Kelner, S. R. and F. A. Aharonian (2008). »Energy spectra of gamma rays, electrons, and neutrinos produced at interactions of relativistic protons with low energy radiation«. In: Phys. Rev. D 78.3, 034013, p. 034013. DOI: 10.1103/PhysRevD.78.034013. arXiv: 0803.0688.

Kelner, S. R., F. A. Aharonian and V. V. Bugayov (2006). »Energy spectra of gamma rays, electrons, and neutrinos produced at proton-proton interactions in the very high energy regime«. In: Phys. Rev. D 74.3, 034018, p. 034018. DOI: 10.1103/PhysRevD.74.034018. eprint: astro-ph/0606058.

Klapdor-Kleingrothaus, H. V. and K. Zuber (1997). *Teilchenastrophysik*. 1st ed. Teubner-Studienbücher. ISBN: 3-519-03094-2.

Krause, M. et al. (2014a). »Feedback by massive stars and the emergence of superbubbles (Corrigendum). II. X-ray properties«. In: A&A 570, C3, p. C3. DOI: 10.1051/0004-6361/201423871e.

– (2014b). »Feedback by massive stars and the emergence of superbubbles. II. X-ray properties«. In: A&A 566, A94, A94. DOI: 10.1051/0004-6361/201423871. arXiv: 1405.0037.

Lallement, R. (2009). »Some Observations Related to the Origin and Evolution of the Local Bubble/Local ISM«. In: Space Sci. Rev. 143, pp. 427–436. DOI: 10.1007/s11214-008-9428-y.

– (2015). »3D maps of the local interstellar medium: searching for the imprints of past events«. In: *Journal of Physics Conference Series*. Vol. 577. Journal of Physics Conference Series, p. 012016. DOI: 10.1088/1742-6596/577/1/012016. arXiv: 1409.6957.

Lallement, R. et al. (1998). »Local Interstellar Cloud(s) Observations with the GHRS«. In: *The Scientific Impact of the Goddard High Resolution Spectrograph*. Ed. by J. C. Brandt, T. B. Ake and C. C. Petersen. Vol. 143. Astronomical Society of the Pacific Conference Series, p. 403.

Lallement, R. et al. (2014). »3D maps of the local ISM from inversion of individual color excess measurements«. In: A&A 561, A91, A91. DOI: 10.1051/0004-6361/201322032. arXiv: 1309.6100.

L'Heureux, J. et al. (1990). »A detector for cosmic-ray nuclei at very high energies«. In: *Nuclear Instruments and Methods in Physics Research A* 295, pp. 246–260. DOI: 10.1016/0168-9002(90)90444-B.

Lipari, Paolo and Silvia Vernetto (2018). »Diffuse Galactic gamma-ray flux at very high energy«. In: Phys. Rev. D 98, 043003, p. 043003. DOI: 10.1103/PhysRevD.98.043003.

Liu, W. et al. (2017). »The Structure of the Local Hot Bubble«. In: ApJ 834, 33, p. 33. DOI: 10.3847/1538-4357/834/1/33. arXiv: 1611.05133 [astro-ph.HE].

Longair, M. S. (1981). *High Energy Astrophysics*. Cambridge et al.: Cambridge University Press. ISBN: 0 521 38374 9.

– (1992). *High Energy Astrophysics*. 2nd ed. Cambridge University Press. ISBN: 0 521 38374 9.

López-Corredoira, M. et al. (2018). »Disk stars in the Milky Way detected beyond 25 kpc from its center«. In: A&A 612, L8, p. L8. DOI: 10.1051/0004-6361/201832880. arXiv: 1804.03064.

Majumdar, S., S. Bharadwaj and T. R. Choudhury (2012). »Constrainingquasar and intergalactic medium properties through bubble detection in redshifted 21-cm maps«. In: MNRAS 426, pp. 3178–3194. DOI: 10.1111/j.1365-2966.2012.21914.x. arXiv: 1111.6354 [astro-ph.CO].

Massaro, F., D. J. Thompson and E. C. Ferrara (2015). »The extragalactic gamma-ray sky in the Fermi era«. In: A&A Rev. 24, 2, p. 2. DOI: 10.1007/s00159-015-0090-6. arXiv: 1510.07660 [astro-ph.HE].

McQuinn, M. (2016). »The Evolution of the Intergalactic Medium«. In: ARA&A 54, pp. 313–362. DOI: 10.1146/annurev-astro-082214-122355. arXiv: 1512.00086.

Meegan, C. et al. (2009). »The Fermi Gamma-ray Burst Monitor«. In: ApJ 702, pp. 791–804. DOI: 10.1088/0004-637X/702/1/791. arXiv: 0908.0450 [astro-ph.IM].

Mészáros, P. (2017). »Astrophysical Sources of High-Energy Neutrinos in the IceCube Era«. In: *Annual Review of Nuclear and Particle Science* 67, pp. 45–67. DOI: 10.1146/annurev-nucl-101916-123304. arXiv: 1708.03577 [astro-ph.HE].

Moralejo, A. (2009). »Status of Magic-II«. In: *ArXiv e-prints*. arXiv: 0912.3673 [astro-ph.IM].

Murase, K. (2015). »Active Galactic Nuclei as High-Energy Neutrino Sources«. In: *ArXiv e-prints*. arXiv: 1511.01590 [astro-ph.HE].

Nieto, M. M. and S. G. Turyshev (2004). »Measuring the Interplanetary Medium with a Solar Sail«. In: *International Journal of Modern Physics D* 13, pp. 899–906. DOI: 10.1142/S0218271804004955. eprint: astro-ph/0308108.

Nieto, M. M., S. G. Turyshev and J. D. Anderson (2005). »Directly measured limit on the interplanetary matter density from Pioneer 10 and 11«. In: *Physics Letters B* 613, pp. 11–19. DOI: 10.1016/j.physletb.2005.03.035. eprint: astro-ph/0501626.

Perl, M. L. et al. (1975). »Evidence for anomalous lepton production in e^+e^- annihilation«. In: *Physical Review Letters* 35, pp. 1489–1492. DOI: 10.1103/PhysRevLett.35.1489.

Poleski, R. (2013). »Transformation of the equatorial proper motion to the Galactic system«. In: *ArXiv e-prints*. arXiv: 1306.2945 [astro-ph.IM].

Povh, B. et al. (2014). *Teilchen und Kerne*. Vol. 9. Springer-Lehrbuch. Berlin: Springer Spektrum. Chap. 10, 11 and 12. ISBN: 978-3-642-37821-8.

Press, W. H. et al. (1992). *Numerical Recipes in Fortran: The Art of Scientific Computing*. 2nd ed. Cambridge University Press. ISBN: 0 521 43064 X.

Reis, W. et al. (2011). »Interstellar Reddening in the Local Bubble and Loop I Region: Insight from Strömgren Photometry Analysis and Three-dimensional Modeling«. In: ApJ 734, 8, p. 8. DOI: 10.1088/0004-637X/734/1/8.

Schild, R. E. et al. (2012). »Why don't clumps of cirrus dust gravitationally collapse?« In: *Physica Scripta Volume T* 151.1, 014084, p. 014084. DOI: 10.1088/0031-8949/2012/T151/014084. arXiv: 1210.1103.

Slavin, J. D. (2017). »Structures in the Interstellar Medium Caused by Supernovae: The Local Bubble«. In: *Handbook of Supernovae, ISBN 978-3-319-21845-8. Springer International Publishing AG, 2017, p. 2287*. Ed. by A. W. Alsabti and P. Murdin, p. 2287. DOI: 10.1007/978-3-319-21846-5_14.

Smith, N. (2014). »Mass Loss: Its Effect on the Evolution and Fate of High-Mass Stars«. In: ARA&A 52, pp. 487–528. DOI: 10.1146/annurev-astro-081913-040025. arXiv: 1402.1237 [astro-ph.SR].

Spanish National Research Council (2017). *Possible explanation for the galaxy's cosmic radiation.* https://phys.org/news/2017-09-explanation-galaxy-cosmic.html. Accessed: 17-11-2018.

Street, J. C. and E. C. Stevenson (1937). »New Evidence for the Existence of a Particle of Mass Intermediate Between the Proton and Electron«. In: *Physical Review* 52, pp. 1003–1004. DOI: 10.1103/PhysRev.52.1003.

Takeda, M. et al. (1999). »Small-Scale Anisotropy of Cosmic Rays above 10^{19} eV Observed with the Akeno Giant Air Shower Array«. In: ApJ 522, pp. 225–237. DOI: 10.1086/307646. eprint: astro-ph/9902239.

Tanabashi, M. et al. (2018). »Review of Particle Physics«. In: *Phys. Rev. D* 98 (3). DOI: 10.1103/PhysRevD.98.030001. URL: https://link.aps.org/doi/10.1103/PhysRevD.98.030001.

The IceCube Collaboration et al. (2015). »The IceCube Neutrino Observatory - Contributions to ICRC 2015 Part II: Atmospheric and Astrophysical Diffuse Neutrino Searches of All Flavors«. In: *ArXiv e-prints*. arXiv: 1510.05223 [astro-ph.HE].

Totsuka, Y. and Super-KAMIOKANDE Collaboration (1998). »Evidence for Neutrino Oscillation from Super-Kamiokande«. In: *19th Texas Symposium on Relativistic Astrophysics and Cosmology*. Ed. by J. Paul, T. Montmerle and E. Aubourg, p. 616.

Unger, M. and Pierre Auger Collaboration (2017). »Highlights from the Pierre Auger Observatory«. In: *International Cosmic Ray Conference* 35, 1102, p. 1102. arXiv: 1710.09478 [astro-ph.HE].

Unsöld, A. and B. Baschek (2002). *Der Neue Kosmos*. Berlin et al.: Springer Verlag. ISBN: 3-540-42177-7.

Watson, A. A. (2014). »High-energy cosmic rays and the Greisen-Zatsepin-Kuz'min effect«. In: *Reports on Progress in Physics* 77.3, 036901, p. 036901. DOI: 10.1088/0034-4885/77/3/036901. arXiv: 1310.0325 [astro-ph.HE].

Wolfenstein, L. (1979). »Neutrino oscillations and stellar collapse«. In: Phys. Rev. D 20, pp. 2634–2635. DOI: 10.1103/PhysRevD.20.2634.

Xu, D. and IceCube Collaboration (2017). »Search for Astrophysical Tau Neutrinos with IceCube«. In: *ArXiv e-prints*. arXiv: 1702.05238 [astro-ph.HE].